

# Weak Interactions between Poly(ether imide) and Carbon Dioxide: A Multiscale Investigation Combining Experiments, Theory, and Simulations

Giuseppe Scherillo, Giuseppe Mensitieri,\* Antonio Baldanza, Valerio Loianno, Pellegrino Musto,\* Marianna Pannico, Andrea Correa,\* Antonio De Nicola, and Giuseppe Milano



Cite This: *Macromolecules* 2022, 55, 10773–10787



Read Online

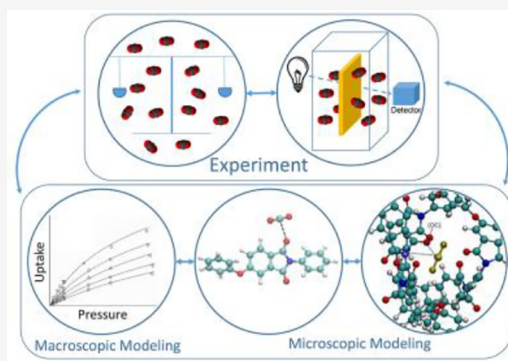
ACCESS |

Metrics & More

Article Recommendations

Supporting Information

**ABSTRACT:** This contribution aims at an understanding, at a molecular scale, of the state of CO<sub>2</sub> molecules absorbed in glassy poly(ether imide) (PEI). This issue has been challenged by combining different approaches that tackle the problem from both the experimental and the theoretical viewpoints and providing a comprehensive physicochemical picture. In situ FTIR spectroscopy and gravimetry were exploited to gather relevant experimental information, while molecular dynamics (MD), density functional theory (DFT), and statistical thermodynamics approaches were used to model the behavior of the binary system at different scales. Based on the findings of FTIR spectroscopy and on DFT and MD calculations, it was determined that, among the possible interaction configurations, some are prevailing. In particular, the carbon atom of carbon dioxide molecules establishes relatively weak interactions prevalently with the carbonyl groups of PEI. A quantitative estimate of such interaction has been provided by MD calculations. The system was also analyzed using a lattice fluid model, specifically developed to deal with sorption of low molecular weight compounds in glassy polymers, that is rooted on statistical thermodynamics, determining the values of the isosteric heat of sorption and carbon-dioxide–polymer interaction energy. Finally, experimental data of CO<sub>2</sub>–PEI mutual diffusivity have been interpreted using a semiempirical theoretical model accounting for the effects of the penetrant concentration, of energy barriers associated with the occurrence of an effective diffusive jump, and of a thermodynamic factor.



## 1. INTRODUCTION

Sorption thermodynamics and mass transport of gases in synthetic polymers is an important subject in view of its scientific fundamental interest and of the considerable industrial impact. This issue has been addressed with experimental tools, with theoretical modeling and with molecular simulations.<sup>1–13</sup> For example, Theodorou and co-workers reported a combined computational and experimental study on the effect of CO<sub>2</sub> adsorption on molten atactic polystyrene properties.<sup>14</sup> The motivation of these studies is the important technological implications, in particular, in the fields of polymeric membranes for separation of gaseous mixtures<sup>15–18</sup> and of barrier polymers for packaging applications.<sup>19</sup>

Poly(ether imide)s are a class of commercial polymers (under the trade names of Matrimid and Ultem) of choice for the realization of hollow fiber membranes employed in separations of CO<sub>2</sub>-containing gas mixtures, in view of their high CO<sub>2</sub> affinity, thermal and chemical stability, easy filmability, and good mechanical properties.<sup>20</sup> Membranes realized with neat poly(ether imide)s or with poly(ether imide)s mixed with inorganic fillers (so-called mixed matrix membranes) find applications in many separation processes involving CO<sub>2</sub>-containing gas mixtures, like biogas upgrad-

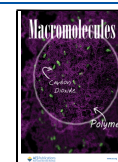
ing,<sup>21</sup> purification of natural gas (gas sweetening),<sup>20</sup> and enhanced oil recovery.<sup>22</sup>

Separation operated by permeation through membranes depends upon the relative values of diffusivity and solubility of the gases composing the mixture. Membrane selectivity and permeability of the components in a mixture are related to molecular level phenomena such as competitive sorption effects. Physical and chemical interactions between gas molecules and the polymer matrix play a major role in determining selectivity due to solubility differences.<sup>23</sup> In this respect, achieving a quantitative understanding and a reliable mathematical description of the interactions between the polymer backbone and carbon dioxide could be beneficial for the rational design of PEI-based membranes for efficient

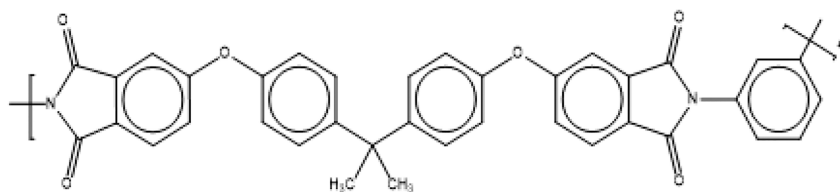
Received: July 5, 2022

Revised: November 6, 2022

Published: December 1, 2022



Scheme 1. Molecular Structure of PEI



separations.<sup>24</sup> See Scheme 1 for the schematic representation of the PEI molecular structure.

Besides the interactions of CO<sub>2</sub> with functional groups in a polymer chain, other relevant factors affecting CO<sub>2</sub> solubility are the steric hindrance effects related to the position of polar groups on the polymer backbone, the number of electron-donating groups, and the morphology of the polymer.<sup>25</sup> Toward the aim of investigating these interactional issues, IR spectroscopy is among the most informative experimental techniques. In fact, it has been successfully employed to characterize H-bonding systems in which the strength of the interaction induces clearly recognizable effects in the probe spectrum, which were exploited to identify and quantify the involved molecular species.<sup>26,27</sup> In the case of weaker interactions as those produced by CO<sub>2</sub>, the perturbation of the probe spectrum is more subtle and more challenging to investigate. Yet, a careful vibrational analysis of the CO<sub>2</sub> fundamental modes will provide experimental evidence of the occurring interactions.

Our group has already performed several investigations focused on sorption thermodynamics of low molecular weight compounds in glassy polymers where modeling of the thermodynamic behavior of the systems was combined with the wealth of information provided by vibrational spectroscopy and gravimetric measurements.<sup>26–30</sup> In all the systems considered, the results of vibrational spectroscopy were used to tailor the structure of the thermodynamic model used to interpret sorption thermodynamics. In particular, the interpretation of experimental sorption isotherms was performed using a statistical thermodynamics approach consisting of the so-called nonequilibrium theory for glassy polymers with nonrandom hydrogen bonding,<sup>31</sup> NETGP-NRHB. This is a model based on a compressible lattice fluid that accounts for the nonequilibrium nature of glassy polymers and possible self- and cross-specific interactions between polymer and penetrant (e.g., hydrogen bonding and Lewis acid/Lewis base interactions). This approach is based on extending to the case of glassy polymers the theoretical framework of the equilibrium NRHB equation of state, EoS,<sup>32,33</sup> originally developed by Panayiotou et al. to deal with rubbery polymers. This extension was performed adopting the procedure introduced by Sarti and Doghieri<sup>34,35</sup> to extend sorption equilibrium theories, based on the EoS, to the case of glassy polymers. The same approach has also been used in the present context. However, due to the weak specific interactions between PEI and CO<sub>2</sub>, the terms that take into account the contribution of the specific interactions have been eliminated from the model, so that the version adopted in the present study is referred to as the NETGP-NR model.

To gather further insight at a molecular level, some systems were also analyzed in the literature by complementing vibrational spectroscopy and statistical thermodynamics models with molecular dynamics (MD) calculations.<sup>26</sup> In the

present contribution we have further extended the multidisciplinary nature of the investigation. With the aim of interpreting the experimental results provided by vibrational spectroscopy and gravimetry for the PEI–CO<sub>2</sub> system, besides the statistical thermodynamic approach (NETGP-NR model) and the MD simulations, we have also employed density functional theory (DFT) calculations to elucidate the interactional energy for the CO<sub>2</sub>–carbonyl adduct. These different approaches provided consistent results in terms of thermodynamic behavior and of relevant thermal features of the polymer–gas mixture. This multidisciplinary methodology is able to deliver a comprehensive and detailed physical picture of the sorption process and provides a useful framework for the design and performance assessment of membranes for gas separations.

## 2. MATERIALS AND METHODS

**2.1. Materials.** Amorphous poly(ether imide) (PEI) films ( $M_n = 1.2 \times 10^4$  Da,  $M_w = 3.0 \times 10^4$  Da, glass transition temperature ( $T_g$ ) = 210 °C, thickness 50.0 μm) were purchased from Goodfellow Co. (Coraopolis, PA, USA). The films were dissolved in chloroform (15 wt %/wt concentration) to be solution cast on a tempered glass support. For film thicknesses exceeding 25 μm a calibrated Gardner knife was used to spread the solution over a glass support; the cast film was subsequently dried for 1 h at room temperature, 1 h at 80 °C, and then overnight at 120 °C. Last, the film was removed from the substrate by immersion in distilled water at 80 °C. The final film thickness was  $56 \pm 4$  μm for the gravimetric measurements and 67.7 μm for the FTIR measurements. Thinner films for FTIR analysis (below 5.0 μm) were prepared via a two-step, spin-coating process performed by a Chemat KW-4A apparatus from Chemat Technologies Inc. (Northridge, CA, USA). Spinning conditions were 12 s at 700 rpm for the first step and 20 s at 1500 rpm for the second step. The spin-coated films were dried in the same conditions as for the thicker films, and freestanding samples were removed in distilled water at room temperature.

The pure polymer density has been measured at 25 °C by flotation in a CaCl<sub>2</sub> water solution, and it is equal to 1.297 g·cm<sup>-3</sup>. The polymer density at other temperatures has been calculated using a value of the thermal expansion coefficient,  $\alpha$ , equal to  $0.56 \times 10^{-4}$  K<sup>-1</sup>.<sup>18</sup>

**2.2. FTIR Spectroscopy.** Spectroscopic analysis of the sorption process was made by a *time-resolved* collection of spectra of PEI films exposed to gaseous carbon dioxide at constant pressure and at controlled temperature. The FTIR measurements were performed under gas flowing using a modified Linkam cell, THMS350 V (Surrey, UK), equipped with temperature control (–180 to 350 °C) and a vacuum system. The cell was operated through service lines connected to a mass-flow controller [MKS type GMS0A (Andover, MA, USA)] for setting the CO<sub>2</sub> flux, while a solenoid valve regulated the pressure inside the cell. The system was equipped with a Pirani vacuumeter and a MKS Baratron 121 pressure transducer (produced by MKS Instruments, Andover, MA, full scale 1000 Torr, resolution 0.01 Torr, accuracy equal to  $\pm 0.5\%$  of the reading).

A schematic representation of the experimental apparatus is reported in ref 36. Differential sorption tests at 35, 27, 18, and 0 °C were performed by increasing stepwise the CO<sub>2</sub> pressure within

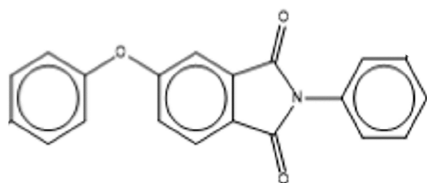
the 40–150 Torr range. Further measurements on the sample equilibrated at 150 Torr were performed in the temperature range 0 to  $-100$  °C. Data collection was made by a Spectrum-100 FTIR spectrometer (PerkinElmer, Norwalk, CT, USA), equipped with a Ge on KBr beam splitter and a wide-band DTGS detector. Instrumental parameters were set as follows: resolution,  $2\text{ cm}^{-1}$ ; optical path difference velocity,  $0.20\text{ cm/s}$ ; number of coadded scans, 32 for equilibrium measurements, 1 for kinetic collections. Full absorbance spectra (i.e., PEI plus sorbed  $\text{CO}_2$ ) were obtained using as background the single-beam spectrum collected on the empty cell at the same temperature and  $\text{CO}_2$  pressure of the test. The spectra representative of absorbed  $\text{CO}_2$  were obtained by difference spectroscopy eliminating the interference of the substrate, i.e.,  $A_D = A_s - A_r$ , where  $A_D$ ,  $A_s$ , and  $A_r$  represent, respectively, the difference spectrum (absorbed  $\text{CO}_2$ ), the sample spectrum (PEI after  $\text{CO}_2$  sorption), and the reference spectrum (fully dried PEI film).

**2.3. Gravimetric  $\text{CO}_2$  Sorption Experiments.** Stepwise sorption experiments have been conducted with a gravimetric apparatus based on a CAHN-D200 microbalance by Thermo Electron Co. (Waltham, MA, USA) working at controlled temperature and gas pressure. The balance has a resolution of  $10^{-7}\text{ g}$  and an uncertainty of  $\pm 3 \times 10^{-7}\text{ g}$ . It is equipped with a measuring chamber whose temperature is controlled by a thermal bath with an uncertainty of  $\pm 0.01$  °C. The whole apparatus is made leak proof with Swagelok fittings. A pumping station combining a turbopump and a membrane backing pump (Pfeiffer HiCUBE 80, ultimate pressure  $10^{-7}\text{ mbar}$ , pumping speed  $35\text{ L}\cdot\text{s}^{-1}$ ) is used to desiccate the polymer specimen before each sequence of sorption steps. Two pressure transducers, MKS Baratron 121 A from MKS Instruments of 100 and 1000 Torr full scale (resolution 0.01% of full scale and an accuracy equal to  $\pm 0.5\%$  of the reading), were used to record the pressure during the experiment. Sorption tests are conducted by drying first the specimen under high vacuum and then by modifying the pressure in the sample chamber stepwise at fixed temperature. The experiments were conducted at temperature values ranging from 0 to  $35$  °C. Both sorption kinetics and the amount of  $\text{CO}_2$  absorbed at phase pseudoequilibrium were collected at each pressure at the various temperatures. Further details about the apparatus can be found in ref 37.

**2.4. DFT Calculations: Computational Details.** Quantum chemical calculations were performed using the DFT by the Gaussian09 package.<sup>38</sup> Electronic configuration of all atoms was described by the 6-31G(d,p) basis set.<sup>39–43</sup> To properly identify  $\text{CO}_2$ –PEI interaction sites and to screen for lower energy level configurations, we tested several starting geometries, performing, first, constrained geometry optimizations, forcing the interaction between  $\text{CO}_2$  and PEI in different binding points and different orientations. The most promising structures were fully optimized, removing all constraints. The M06L functional was employed for both geometry optimizations and vibrational calculations. Minnesota functionals are well known to reproduce very well noncovalent interactions and weakly bound complex geometries.<sup>44,45</sup> According to the level of theory employed, IR frequencies were scaled by 0.950.<sup>46</sup>

The PEI molecular model was selected to be able to simulate the relevant functional groups with the associated molecular environment. The model consists of a section of a single PEI monomeric unit; see Scheme 2.

### Scheme 2. PEI Molecular Model Adopted in DFT Calculations<sup>a</sup>



<sup>a</sup>Hydrogen atoms are omitted.

If not indicated otherwise, all interaction energies,  $E_{int}$ , herein reported were calculated as differences between the product energy and the reactants' total energy (see Supporting Information), and all interaction energies were corrected for basis set superposition error (BSSE correction) with the counterpoise approach of Boys and Bernardi.<sup>47</sup> Negative values for  $E_{int}$  mean stable PEI/ $\text{CO}_2$  adducts. All geometries reported in this paper were fully optimized. Vibrational analysis shows no imaginary frequencies for all reported minima.

**2.5. Molecular Dynamics: Computational Details.** To model PEI chains and  $\text{CO}_2$ , we adopted the OPLS-AA force-field.<sup>48,49</sup> In the Supporting Information, SI, the full list of used parameters for bonded and nonbonded interactions is reported. In Scheme S1, the chemical skeleton of the PEI repeating unit is reported together with atom type tags. For all simulated systems, a PEI chain is composed of 12 repeating units. A phenyl group and a hydrogen atom are used as the chain's terminals. A pre-equilibration procedure to obtain a well-equilibrated polymer melt structure is achieved by following the procedure reported by De Nicola<sup>50,51</sup> using subsequent relaxations using the hybrid particle-field (hPF) method.<sup>52,53</sup> In particular, hPF simulations have been performed in an NVT ensemble by using the OCCAM package.<sup>54</sup> For all hPF simulations a time step of 1 fs has been employed. The temperature has been kept constant at 570 K by using the Andersen thermostat<sup>55</sup> with a collision frequency of  $7\text{ ps}^{-1}$ . The density field update frequency was set to 1 ps. A more detailed description of the relaxation procedure can be found in ref 50. The basics of the hPF simulation method employed here can be found in refs 52 and 53. The relaxed polymer bulk configuration, obtained by hPF simulations, has been used as an initial coordinate set for standard atomistic MD.

To test the accuracy of our modeling approach in describing the dynamics of polymer chains for the case of neat PEI and of a PEI matrix containing absorbed  $\text{CO}_2$  molecules, additional calculations have been performed aimed at the evaluation of the  $T_g$  of the proposed atomistic model of PEI, as determined by the location of the change of slope in the density–temperature curve.<sup>56–60</sup> Three systems have been considered: neat PEI, a PEI matrix containing 0.2004 g  $\text{CO}_2$ /100 g PEI, and a PEI matrix containing 0.8064 g  $\text{CO}_2$ /100 g PEI. A series of constant-NPT MD simulations are performed at different temperatures (each system was cooled from 700 K stepwise to 300 K by decrements of 50 K), and the equilibrium density was recorded for each of them. Full details of the adopted procedure along with relevant results obtained are reported in Section S2 of the SI (in the same section is also shown the agreement of model predictions with experimental X-ray scattering intensities of neat PEI at 308 K). The results of calculations give an estimation of  $T_g$  of  $494 \pm 4\text{ K}$ ,<sup>59</sup> thus providing an indirect mean of validation of the accuracy of representation of polymer chain dynamics. It is worth noticing that, from the performed calculations, the predicted values of  $T_g$  of PEI– $\text{CO}_2$  systems with a mass fraction of  $\text{CO}_2$  equal to 0.02 and 0.08 are indistinguishable from those predicted for neat PEI, indicating that the dynamics of polymer chains is unaffected by the presence of the amounts of  $\text{CO}_2$  considered in the present investigation.

According to the experimental gas concentrations, corresponding to the sorption isotherm obtained at 308.15 K and reported in Figure 7, a certain number of  $\text{CO}_2$  molecules have been randomly inserted in the pre-equilibrated PEI matrix by using the Packmol package.<sup>61</sup> In total, four systems have been prepared (system compositions are reported in Table 1). All atomistic simulations (PEI and PEI/ $\text{CO}_2$ ) have been performed in the NPT ensemble by using the GROMACS package.<sup>62</sup> A time step of 2 fs was used for all simulations. The nonbonded interactions modeled by Lennard-Jones potentials were truncated after a cutoff of 1.1 nm, while the Coulomb long-range interactions were treated by generalized reaction-field ( $\epsilon_{rf} = 5$ , cutoff 1.1 nm). The temperature of the systems was controlled, at 308.15 K, using the Berendsen thermostat,<sup>63</sup> with a characteristic coupling time  $\tau = 0.2\text{ ps}$ . The pressure was kept constant at 1 atm using the Berendsen barostat ( $\tau_p = 2.0\text{ ps}$ ).<sup>63</sup> All bonds involving hydrogens have been constrained by using the LINCS algorithm.<sup>64</sup> For all PEI



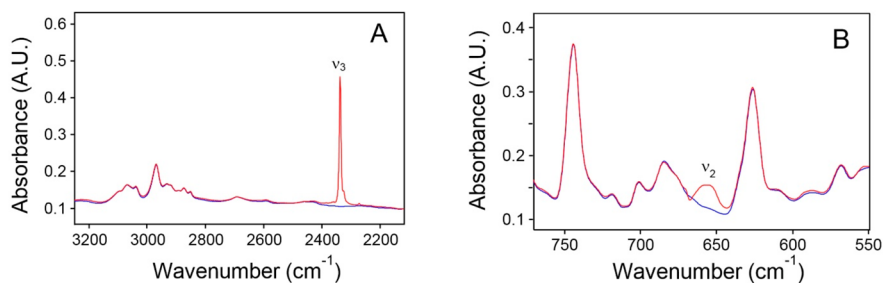


**Figure 1.** Absorbance spectra in the 3250–2150  $\text{cm}^{-1}$  range (A) and in the 770–550  $\text{cm}^{-1}$  range (B) of the fully dried PEI (blue trace) and of PEI equilibrated at 150 Torr of  $\text{CO}_2$  pressure. Both spectra were collected at  $-50^\circ\text{C}$  on a 2.6  $\mu\text{m}$  thick film.

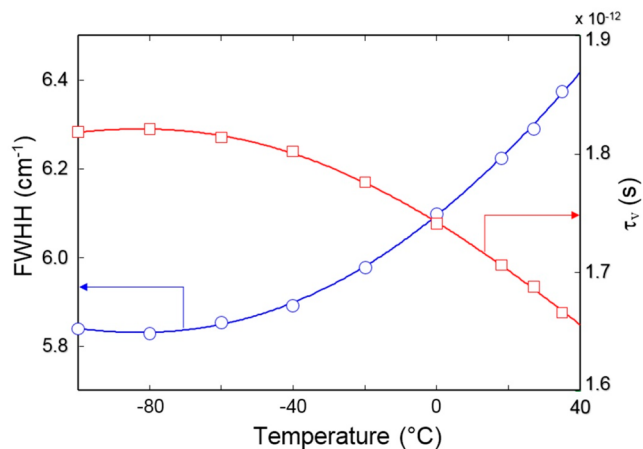


**Figure 2.** fwhh and relaxation time,  $\tau_v$ , as a function of temperature in the  $-100$  to  $35^\circ\text{C}$  range.

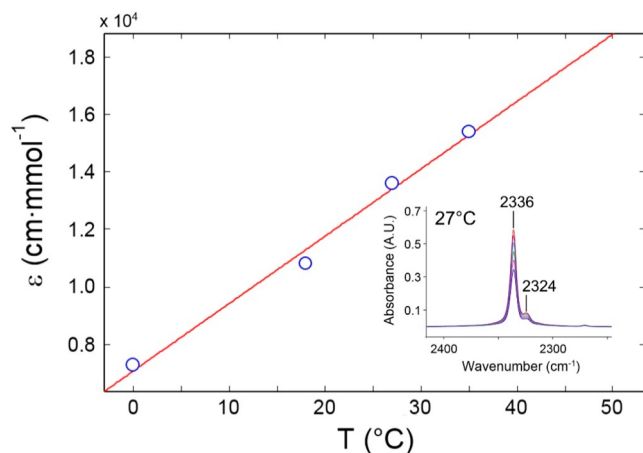


**Figure 3.** Integrated molar absorptivity,  $\epsilon$ , as a function of temperature in the  $0$ – $35^\circ\text{C}$  interval. The inset displays the analytical signal ( $\nu_3$ ) in the explored pressure range at  $27^\circ\text{C}$ .

systems including  $\text{CO}_2$  molecules, a pre-equilibration run of 15 ns was followed by a production run of 600 ns, as indicated in Table 1.

**2.6. NR and NETGP-NR Models: Description of Sorption Thermodynamics and Relevant Thermal Properties.** Nonequilibrium thermodynamics of glassy polymers (NETGP)<sup>34,35</sup> is a theoretical framework rooted upon the thermodynamics of systems with internal state variables<sup>65–69</sup> aimed at describing sorption thermodynamics of low molecular weight compounds in glassy polymers. It is based on the extension of equilibrium thermodynamics models to the case of pseudoequilibrium between an equilibrium multicomponent penetrants fluid phase (where, generally, the polymer is assumed not to be present) and the corresponding

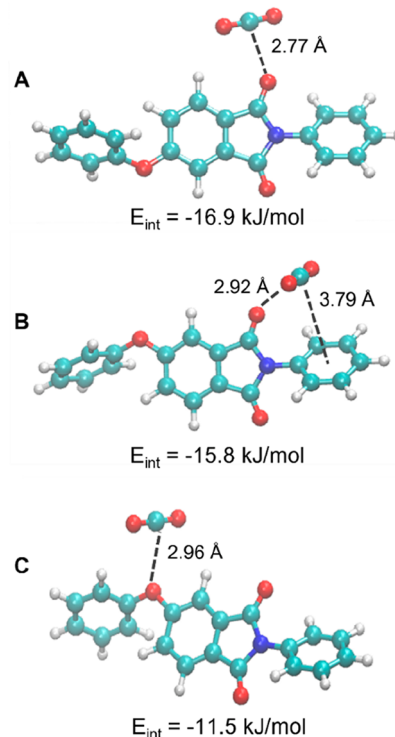


**Figure 4.** Fully optimized structures for PEI/ $\text{CO}_2$  complexes. Hydrogen atoms are in white, carbon atoms are in gray, oxygens are in red, and nitrogen atoms are in blue. Important distances and corresponding interaction energies are also reported.

polymer-penetrants phase locked in an out-of-equilibrium “glassy” state. In the present contribution, we adopt the NETGP procedure to extend the NRHB compressible lattice fluid (LF) model,<sup>32,33</sup> obtaining a theoretical framework to be used to interpret the thermodynamics of glassy polymer–absorbed gas systems. The corresponding NETGP-NRHB model<sup>27,31</sup> accounts for the non-randomness of distribution of mean-field contacts and voids within the lattice and for possible occurrence of strong specific interactions, e.g., hydrogen bonding and Lewis acid/base interactions.

For the PEI– $\text{CO}_2$  system under investigation, vibrational spectroscopy analysis, molecular dynamics simulations, and ab initio calculations, also reported in the present contribution, provide evidence for disregarding the occurrence of hydrogen bonding (HB) interactions, as well as of other specific interactions, in the implementation of the model. Based on this indication, to interpret PEI– $\text{CO}_2$  data we have adopted a simplified version of the NETGP-NRHB model that does not account for specific interactions, which is here referred to as the NETGP-nonrandom (NETGP-NR) model. It is based on the general nonequilibrium expression of the Gibbs energy obtained by extending the corresponding NRHB equilibrium model

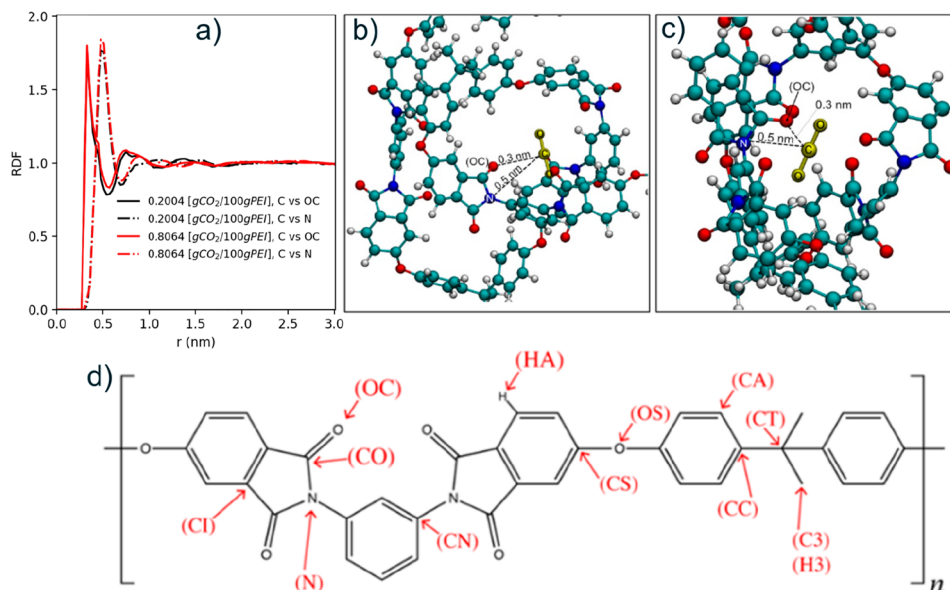


**Figure 5.** (a) Comparison between RDFs calculated at 303.15 K for C–OC (black lines) and C–N (red lines) pairs calculated for systems at 0.2004 and 0.8064 CO<sub>2</sub> mass fractions. In panels (b) and (c) two representative snapshots showing the distance between the carbon atom C (CO<sub>2</sub>) and atom types OC and N (imide groups) are reported. The carbon dioxide molecule is reported in yellow to highlight its position. Only a single chain of PEI, interacting with a carbon dioxide molecule, is reported for simplicity. The OC and N type interacting with CO<sub>2</sub> are labeled, while for the remaining PEI chain the atom color code is blue (nitrogen), white (hydrogen), cyan (carbon), and red (oxygen). (d) Chemical structure of a PEI repeating unit. Atom types are indicated by arrows (red text in brackets). For clarity, the hydrogen atoms are omitted except for the ones used for the labeling. The label C is used for the carbon atom of carbon dioxide.

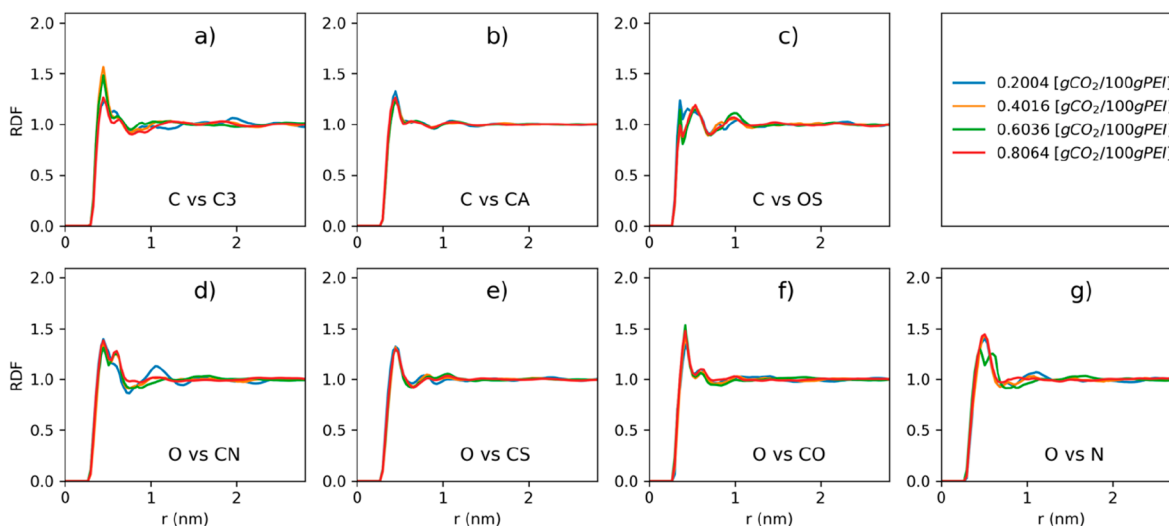


**Figure 6.** RDFs calculated at 308.15 K for the carbon and oxygen atoms of carbon dioxide with respect to PEI's functional groups (these sites are defined as center of mass of the corresponding functional group). Four different concentrations of CO<sub>2</sub> in PEI have been considered. RDFs have been calculated by time averaging the last 100 ns of the production runs.

without the HB contribution (referred to as the equilibrium NR model).

The phase equilibrium between an external multicomponent fluid phase (a mixture of penetrant in the liquid or vapor state), in which the polymer is assumed to be not soluble, and a condensed glassy polymer phase containing adsorbed penetrant molecules can be described by imposing the equivalence of chemical potentials of the penetrants in the two phases. The chemical potentials of the penetrants within the fluid phase can be described by the equilibrium NR model, while the chemical potentials of the penetrants within the polymer phase are expressed in terms of the NETGP-NR model.<sup>27</sup> This is a pseudophase equilibrium in view of the nonequilibrium state of the polymer phase.

The corresponding set of equations that dictates the pseudoequilibrium condition is

$$\mu_i^{\text{IE}}(T, \vec{n}, \rho_p) = \mu_i^{\text{eq}}(T, P, n_1, n_2, \dots, n_t) \quad (1)$$

In eq 1 the number of penetrants is  $t$ , the total number of components, including also the polymer species, is  $t + 1$ , and  $\vec{n} \equiv (n_1, n_2, \dots, n_{t+1})$  is a vector of variables, each component of this vector representing the number of moles of every component. The symbol  $\mu_i^{\text{IE}}(T, \vec{n}, \rho_p)$  represents the chemical potential of penetrant  $i$  within the polymer phase calculated using the NETGP-NR model. The superscript IE (“instantaneous equilibrium”) refers to a relevant assumption made in the development of the NETGP-NR model:

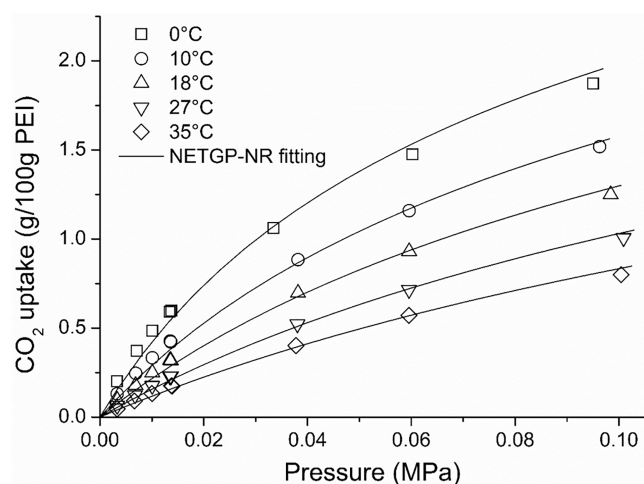


**Figure 7.** Experimental sorption isotherms of CO<sub>2</sub> in PEI at several temperatures. Continuous lines represent the best fitting results obtained using the NETGP-NR model.

**Table 1.** MD Simulated Systems at Different Concentrations of CO<sub>2</sub><sup>a</sup>

CO <sub>2</sub> mass/ PEI mass × 100	no. of PEI chains	no. of CO <sub>2</sub>	no. of particles	aver. box size (X, Y, Z) [nm]	time [ns]
0.2004	108	31	90 813	12.67 × 12.69 × 6.34	600
0.4016	108	71	90 933	12.63 × 12.73 × 6.38	600
0.6036	108	101	91 023	12.63 × 12.76 × 6.36	600
0.8064	108	141	91 143	12.65 × 12.73 × 6.38	600

<sup>a</sup>The concentration as mass of CO<sub>2</sub>/mass of polymer × 100.

although a nonequilibrium value for polymer density is imposed, it is assumed that the number of pair contacts in the lattice is calculated using the equilibrium expressions (see the SI file for further details on this point). The symbol  $\mu_i^{\text{IE}}(T, P, n_1, n_2, n_i)$  represents the chemical potential of penetrant  $i$  within the external multicomponent fluid phase calculated using the equilibrium NR model. It is worth noting that  $\mu_i^{\text{IE}}$  does not depend upon pressure (see the SI file). This is a relevant result of the classical development of NETGP theory (see refs 27 and 34).

More details on the NR and NETGP-NR models, on the mathematical expressions provided for the chemical potentials, on the related assumptions, and on the model parameters are reported in the SI file.

For the system under investigation the glassy polymer is contacted with only one penetrant, so that the external phase is pure gaseous CO<sub>2</sub>, while the polymer phase is a binary mixture (for the binary mixture at hand we use the subscript “1” to refer to CO<sub>2</sub> and the subscript “p” to refer to PEI). Equation 1 has been used to interpret experimental sorption isotherms of carbon dioxide in poly(ether imide) at several temperatures determining the values of the two binary interaction parameters,  $k_0$  and  $a_T$  (see the SI file for details), from the fitting of the experimental data. Once the parameters have been estimated, the equations of the NETGP-NR model have been then used to predict some relevant thermal and interactional properties. In fact, we have estimated, using this model, the isosteric heat of sorption of CO<sub>2</sub>,  $\Delta H_{\text{CO}_2}^{\text{ISOST}}$ , in PEI (to be compared with its value determined from experimental sorption isotherms) and the interaction energy of an adsorbed molecule of CO<sub>2</sub> with the surrounding polymer matrix (to be compared with its value estimated by DFT calculations).

A theoretical estimate of the isosteric heat of sorption of a pure gas in a glassy polymer can be obtained based on the following equation (see the SI file for details):

$$\Delta H_1^{\text{ISOST}} = H_{1,\delta}^{\text{eq}}(T, P) - \bar{H}_1^{\text{IE}}(T, \bar{n}, \rho_p) \quad (2)$$

where  $H_{1,\delta}^{\text{eq}}$  represents the corresponding equilibrium molar enthalpy of the pure penetrant phase at a given pressure  $P$  and temperature  $T$ . Its value is provided by the NR model (see the SI file) as applied to the pure component case.  $\bar{H}_1^{\text{IE}}$  represents the partial molar enthalpy of the adsorbed gas and can be calculated from

$$\bar{H}_1^{\text{IE}} \equiv \left( \frac{\partial H^{\text{IE}}}{\partial n_1} \right)_{P, T, \rho_p, n_p} = \mu_1^{\text{IE}} + T \left( \frac{\partial S^{\text{IE}}}{\partial n_1} \right)_{T, \rho_p, n_p} \quad (3)$$

The values of  $\mu_1^{\text{IE}}$  and of  $\left( \frac{\partial S^{\text{IE}}}{\partial n_1} \right)_{T, \rho_p, n_p}$  can be calculated using the NETGP-NR theory (see the SI for details). An independent estimate of  $\Delta \bar{H}_1^{\text{ISOST}}$  can be obtained based on experimental sorption data collected at low pressure. In fact, in such conditions, since the gas-phase fugacity coefficient can be set equal to unity (ideal gas limit) and the gas-phase excess enthalpy difference, i.e.,  $H_T^{\text{E}}(T, P) - H_T^{\text{E}*}(T, P = 1 \text{ atm})$ , can be neglected, the following expression (see ref 70 and also the SI) holds:

$$\Delta H_1^{\text{ISOST}} = RT^2 \left( \frac{\partial \ln P}{\partial T} \right)_{c_1^g} \quad (4)$$

$P$  and  $T$  are, respectively, the values of temperature and pure gas pressure at which the absorption experiment is performed, while  $c_1^g$  represents the amount of gas absorbed in the polymer phase. In the present contribution, the term  $\left( \frac{\partial \ln P}{\partial T} \right)_{c_1^g}$  is calculated re-elaborating the experimental sorption isotherms, with no need of specifying any functional form for the chemical potentials.<sup>70</sup>

The NETGP-NR model can be used also to evaluate theoretically the interaction energy of an adsorbed CO<sub>2</sub> molecule with the surrounding glassy PEI matrix. In a binary system, the mean-field interaction energy per mole of penetrant in the limit of infinite dilution,  $E_{1p,0}$ , can be estimated using the NETGP-NR model once the binary interaction parameters,  $k_0$  and  $a_T$ , have been determined from the fitting of experimental sorption isotherms. In fact, it can be demonstrated (see the SI for details) that

$$E_{1p,0} = \varepsilon_{1p} \lim_{N_1 \rightarrow 0} \frac{\Gamma_{1p}^{\text{IE}}}{N_1} z N_1 q_1 \Theta_p = \varepsilon_{1p} \lim_{x_1 \rightarrow 0} z \Gamma_{1p}^{\text{IE}} q_1 \Theta_p \quad (5)$$

where  $\varepsilon_{1p}$  represents the mean-field interaction per each LF contact between a segment of species 1 and a segment of species  $p$ ,  $N_1$  represents the number of molecules of penetrant in the penetrant–polymer mixture,  $\Gamma_{1p}^{\text{IE}}$  is the nonrandomness factor (see the SI for details) for the contacts between a segment of species 1 and a segment of species  $p$  under “instantaneous equilibrium” conditions, and  $z q_1$  represents the total number of external contacts for a molecule of species 1 (the parameter  $q_1$  accounts for the structure of the molecules of species 1 within the lattice, in terms of its subdivision in  $r_1$  segments). The factor  $z N_1 q_1$  represents the total number of external contacts of species 1 within the lattice. Finally,  $\Theta_p$  represents the ratio between the total number of contacts of species  $p$  and the total number of contacts within the lattice, which in turn provides, in the case of a random distribution of LF contacts, the probability that a contact involves the species  $p$ . The limit present in eq 5 has been calculated numerically.

The theoretical calculation of  $E_{1p,0}$  can be then performed using eq 5 once  $\Gamma_{1p}^{\text{IE}}(x_1, T, \rho_p)$  is known from the NETGP-NR model.

**2.7. Modeling Mutual Diffusivity in a Glassy Polymer–Penetrant Binary System.** In the limit of low penetrant concentrations in a rubbery polymer, a Fickian diffusive behavior<sup>71–75</sup> is generally observed. Therefore, in a sorption experiment of a penetrant in polymer slab (one-dimensional geometry, binary case) the following equation describes the sorption kinetics:<sup>71</sup>



$$\frac{M(t) - M_0}{M_\infty - M_0} = 1 - \sum_{n=0}^{\infty} \frac{8}{(2n+1)^2 \pi^2} \exp\left(-\frac{D_{12}(2n+1)^2 \pi^2 t}{L^2}\right) \quad (6)$$

where  $M_0$  is the initial mass of the penetrant present within the polymer (uniform concentration),  $M(t)$  is the penetrant mass present within the polymer at time  $t$ ,  $M_\infty$  is the asymptotic value of penetrant mass present at infinite time,  $L$  represents the thickness of the sample slab, and  $D_{12}$  is the so-called mutual diffusivity, assumed to be independent of penetrant concentration (the so-called “ideal Fickian” behavior). The sorption experiment modeled by eq 6 is performed starting from an initial uniform concentration within the slab that is in equilibrium with the external fluid phase. At the start of the experiment, the pressure of the external fluid phase is stepwise increased to a higher value, thus determining the start of the diffusion process of the penetrant within the polymer. The concentration of the penetrant thus reaches, at the end of the sorption process, a new uniform equilibrium concentration. A fingerprint of the ideal Fickian behavior is the linear dependence of  $\frac{M(t)}{M_\infty}$  vs  $\sqrt{t}$  up to  $\frac{M(t)}{M_\infty} \cong 0.5$  with a slope that does not depend on penetrant concentration.

In the case of glassy polymers, mutual diffusivity is dependent on concentration even at low concentrations.<sup>69,70</sup> However, one can still use eq 6 to interpret sorption kinetics provided that the change in concentration during the sorption run is not too high (this type of behavior is generally referred to as “nonideal Fickian” behavior). In such a case, one can assume that the mutual diffusivity is roughly constant during each sorption step. The value of  $D_{12}$  that one gathers from fitting of the sorption curve thus represents an average of the values corresponding to the uniform initial and final penetrant concentration. This average value of diffusivity can be associated with the mean value of concentration (arithmetic average of the initial and final values of uniform concentration). In the present investigation step sorption experiments have been performed at different values of temperature. It was then possible to determine the dependence of mutual diffusivity on penetrant concentration and temperature.

The mutual diffusivity coefficient,  $D_{12}$ , in a penetrant–rubbery polymer binary system can be expressed<sup>76–81</sup> in terms of the so-called *intradiffusion* coefficient of the penetrant,  $D_{1p}$ , that represents the intrinsic mobility of penetrant in a binary mixture in the case of a null value of the gradients of the chemical potentials of the two components:

$$D_{12} = D_{1p} = \frac{D_{1p} \hat{V}_p \rho_1 \left( \frac{\partial \mu_1}{\partial \rho_1} \right)_{T,P,\rho_p}}{RT} \quad (7)$$

This equation holds true not only at small penetrant concentrations but also over a major portion of the concentration interval of the binary system.<sup>76,77</sup> In eq 7  $\hat{V}_p$  is the partial mass volume of the polymer in the mixture.

In the case of a glassy polymer, eq 7 still holds<sup>76,77</sup> but the “thermodynamic factor”,  $\left( \frac{\partial \mu_1}{\partial \rho_1} \right)_{T,P,\rho_p}$ , is now calculated numerically on

the basis of the NETGP-NR model (i.e., as  $\left( \frac{\partial \mu_1^{\text{IE}}}{\partial \rho_1} \right)_{T,P,\rho_p}$ , where the

expression of  $\mu_1^{\text{IE}}$  is provided by eq S19 coupled with eqs S8 and S15, reported in the SI file. In the limit of low concentration of penetrant in a glassy polymer,  $\hat{V}_p$  is approximately equal to  $1/\rho_p$  (where  $\rho_p$  is the nonequilibrium polymer density) since the partial mass volume of the penetrant can be assumed to be equal to zero. Equation 7, where the mutual diffusivity coefficient depends upon a “thermodynamic factor” provided by the NETGP-NR theory, is referred to in the following as NETGP-NR-DM (where DM stands for “diffusion model”).

Inspired by the Cohen–Turnbull expression for the *self*-diffusion coefficient in the case of a one-component fluid,<sup>76</sup> we have adopted for the *intradiffusion* coefficient,  $D_{1p}$ , of a penetrant in a binary glassy polymer–penetrant mixture the following simple empirical law:

$$D_{1p} = D_{00} \exp\left(-\frac{E_d - \sigma_c c}{RT}\right) = D_{00} \exp\left(-\frac{E_d}{RT}(1 - \alpha c)\right) \quad (8)$$

with  $\alpha = \sigma_c/E_d$ . In eq 8  $D_{00}$  and  $E_d$  represent, respectively, a constant pre-exponential factor and a constant activation energy term that accounts for energetic barriers (related to the polymer–penetrant interactions and to the cohesive energy of polymer molecules) to be overcome to realize an effective diffusive jump of a penetrant molecule, while  $\sigma_c$  represents a term accounting for the effect of penetrant concentration ( $c$  [mass of CO<sub>2</sub>/mass of polymer]) on the intrinsic penetrant mobility in the binary mixture. In principle, these three constant parameters only depend on the nature of the components of the binary mixture, and their values can be retrieved from a nonlinear fitting of the experimental  $D_{12}$  data, using eqs 7 and 8.

### 3. RESULTS AND DISCUSSION

**3.1. FTIR Spectroscopy.** In Figure 1A,B are reported the spectra of a fully dried film of PEI (blue traces) and of the same film equilibrated at  $-50$  °C under a CO<sub>2</sub> pressure of 150 Torr (red traces). The antisymmetric stretching mode of CO<sub>2</sub> ( $\nu_3$ ) produces an intense signal at 2336 cm<sup>-1</sup> in an interference-free region, which is well suited for quantitative analysis and for getting information at the molecular level (see Figure 1A). The bending mode ( $\nu_2$ ) is found at around 655 cm<sup>-1</sup> but is weaker and partially overlapped to polymeric bands (see Figure 1B). The intensity of the  $\nu_3$  peaks is linearly correlated to the CO<sub>2</sub> concentration in the polymer according to the Lambert–Beer law, as shown in Figure S1 of the SI file. The isotherm evaluated spectroscopically at 35 °C in the range 0–160 Torr is reported in Figure S2 of the SI file.

*Time-resolved* FTIR measurements allow one to monitor the sorption/desorption kinetics. At 35 °C and 70 Torr of CO<sub>2</sub> pressure, the behavior is Fickian (see Figures S3A and S4 of the SI file for the kinetics measurements based on the signal corresponding to the stretching mode of CO<sub>2</sub> ( $\nu_3$ )); as expected, at 0 °C under the same pressure, the process slowed down (Figures S3B, S4 of the SI file). Comparing the sorption and desorption kinetics (Figures S5 of the SI file) it is noted that at 35 °C they are coincident, which is indicative of a host/guest system with no or very weak interactions. Conversely, at 0 °C a significant hysteresis is observed suggesting a strengthening of the PEI/CO<sub>2</sub> interactions at this temperature that promote the dependence of CO<sub>2</sub> diffusivity on concentration (the value increases with concentration).

Further information on the host/guest interactions can be gathered from the spectra of the probe and the substrate. Considering first the antisymmetric stretching of CO<sub>2</sub>, it is known that, according to the theory of vibrational line shapes, the profile of this transition can be described by the sum of a Gaussian and a Lorentzian band shape, both centered at the peak maximum. The two-component profile is evident in systems with no molecular interactions.<sup>80</sup> In the case of a collisional relaxation mechanism, this complex band shape is due to the probe dynamics, in particular to free rotation in the early stages of the relaxation process, producing the Gauss component and a faster decay at later stages, giving rise to the Lorentz band. Whenever a Gaussian component is evident, a significant free-rotation regime exists, which, in turn, indicates that the probe interrogates a poorly or noninteractive environment with a sizable free volume.<sup>81</sup> In the present case, the  $\nu_3$  vibration produces a sharp, highly symmetrical peak centered at 2336 cm<sup>-1</sup> plus a satellite band partially resolved at 2324 cm<sup>-1</sup>. The latter is a nonfundamental

vibration [ $a(\nu_3 + \nu_2) - \nu_2$  hot-band enhanced by Fermi resonance] and does not originate from a  $\text{CO}_2$  population other than that producing the main signal. Regressing the experimental profile with a standard line shape model,<sup>82</sup> it is found that the  $2336\text{ cm}^{-1}$  component is reproduced with high accuracy by a single Lorentz function, while the weaker band at  $2323\text{ cm}^{-1}$  is better simulated by a Gaussian band shape. The results of the curve-fitting analysis are reproduced in Figure S6 of the SI file. Vibrational relaxation may occur through numerous mechanisms, among which are inter- or intramolecular vibrational energy transfer, energy transfer by collision, and vibrational dephasing from stochastic modulation.<sup>83,84</sup> It has been shown that for the case of the  $\nu_3$  mode of  $\text{CO}_2$  dissolved in water the vibrational relaxation time  $\tau_v$  can be derived from the full width at half-height (fwhh) of the band according to<sup>85,86</sup>

$$\tau_v = \frac{1}{\pi c \times \text{fwhh}} \quad (9)$$

At  $35\text{ }^\circ\text{C}$  the relaxation time is  $1.65\text{ ps}$ : it increases linearly on going from  $35$  to  $-40\text{ }^\circ\text{C}$  and reaches a plateau value of  $1.82 \pm 0.01\text{ ps}$  in the  $-60$  to  $-100\text{ }^\circ\text{C}$  interval (see inset of Figure 2). The value at  $35\text{ }^\circ\text{C}$  is fast compared to collisional relaxation or dephasing processes, whose  $\tau_v$  values typically range between  $5$  and  $10\text{ ps}$  at ambient temperature.<sup>84,87</sup> This result suggests a more efficient energy transfer process, in particular a vibrational mode coupling.<sup>87</sup> For  $\text{CO}_2$  dissolved in water the  $\tau_v$  was estimated to be  $1.0\text{ ps}$  at  $27\text{ }^\circ\text{C}$  and showed an analogous decreasing trend with temperature, although the analysis was performed in the  $27$ – $250\text{ }^\circ\text{C}$  range.<sup>86</sup> The observed behavior was attributed to the direct association of  $\text{H}_2\text{O}$  with  $\text{CO}_2$  molecules, which activates a vibrational coupling path toward energy relaxation. The same mechanism can be invoked in the present case, confirming the occurrence of a molecular interaction between the probe and a functional group on the polymer backbone. The band shape consisting of a single, sharp Lorentzian strongly suggests that, within the sensitivity limit of the technique, all the absorbed  $\text{CO}_2$  molecules are interacting and that the interaction is specific, i.e., involves only a given functional group of the polymer.

The direct association of  $\text{CO}_2$  molecules with PEI binding sites is further confirmed by the analysis of the  $\nu_2$  mode. For the isolated molecule this vibration is degenerate, but, in the case of association, distortion of the linear  $\text{O}=\text{C}=\text{O}$  structure removes the original  $D_{\infty h}$  symmetry and activates in-plane and out-of-plane vibrations. In this situation, the signal splits in two components, providing a clear signature of the occurring interaction. In Figure S7A, of the SI file, is reported the  $\nu_2$  band of  $\text{CO}_2$  in PEI for spectra collected at sorption equilibrium in the temperature range  $35$  to  $-50\text{ }^\circ\text{C}$ . For comparison, Figure S7B, of the SI file, displays the  $\nu_2$  mode of  $\text{CO}_2$  absorbed in a noninteracting medium (ethylene-propylene copolymer). The splitting effect in the PEI/ $\text{CO}_2$  system is evident, while a single, symmetrical profile is observed in the absence of interactions. It has been demonstrated<sup>88–91</sup> that the degree of splitting of the  $\nu_2$  mode (i.e., the difference between the frequencies of the two components,  $\Delta\nu = \nu_2' - \nu_2''$ ) is a sensitive measure of the interaction strength. In PMMA, where a Lewis acid–Lewis base (LA–LB) interaction involving the oxygens of the backbone carbonyls (LB) and the carbon atom of  $\text{CO}_2$  (LA) was assumed,  $\Delta\nu$  amounts to  $8\text{ cm}^{-1}$ . Likewise,  $\Delta\nu$  is  $7.7\text{ cm}^{-1}$  for poly(butyl methacrylate),  $7.9\text{ cm}^{-1}$  for poly(vinyl acetate), and  $4.7\text{ cm}^{-1}$  for poly(vinyl fluoride); that is, it decreases as the

interactions (the Lewis base sites of the polymer) get weaker. In the present system, the spectroscopic signatures point to an analogous interaction mechanism, involving the imide carbonyls as LB. The  $\nu_2$  components were resolved by an LSCF analysis and provided a  $\Delta\nu$  value of  $6.5\text{ cm}^{-1}$ , revealing an interaction strength lower than in PMMA, whose  $\Delta H$  was estimated to be  $1.0\text{ kcal/mol}$ .<sup>88</sup> The lower LB character of the imide carbonyls compared to those in PMMA is to be ascribed to the extensive conjugation of the  $\text{C}=\text{O}$  bond in the substituted phthalimide structure. For the same reason, phthalimide carbonyls are among the weakest proton acceptors in H-bonding interactions.<sup>89</sup>

The involvement of the PEI carbonyls was further confirmed by the *red-shift* of both in-phase and out-of-phase  $\nu(\text{C}=\text{O})$  modes in the presence of  $\text{CO}_2$ , which is caused by a decrease of the carbonyl force constant. The effect is very subtle (maximum shift =  $-0.25\text{ cm}^{-1}$ ) and is best appreciated by difference spectroscopy (DS). In Figure S8, of the SI file, is reported the DS spectrum collected at  $-50\text{ }^\circ\text{C}$ , which evidences the *red-shift* signature, i.e., two first-derivative features centered at  $1779$  and  $1726\text{ cm}^{-1}$ . The difference spectrum is featureless in the remaining frequency range, suggesting that ether oxygens (at  $1238$  and  $1215\text{ cm}^{-1}$ ),<sup>26</sup> albeit potentially interactive, remain unperturbed. This observation confirms the specific character of the  $\text{C}=\text{O}/\text{CO}_2$  interaction.

The molar absorptivity,  $\epsilon$ , of the  $\nu_3$  mode was measured in the temperature range  $0$ – $35\text{ }^\circ\text{C}$  by combining the spectroscopic and the gravimetric isotherms (Figure 3). At  $27\text{ }^\circ\text{C}$   $\epsilon$ , evaluated in terms of absorbance area, was  $1.36 \times 10^4\text{ cm}^2/\text{mmol}$ , in good agreement with the value for  $\text{CO}_2$  dissolved in water ( $1.58 \times 10^4\text{ cm}^2/\text{mmol}$ ).<sup>86</sup> In terms of peak height, the present value of  $1.30 \times 10^6\text{ cm}^2/\text{mol}$  is to be compared to  $0.9 \times 10^6$  and  $1.5 \times 10^6\text{ cm}^2/\text{mol}$  reported, respectively, in refs 86 and 90.

A significant temperature dependence was observed, described by the linear relationship

$$\epsilon(\text{cm}^2/\text{mmol}) = (234 \pm 79) \times T(^{\circ}\text{C}) - (7 \pm 1.8) \times 10^3; R^2 = 0.988 \quad (10)$$

It is explicitly noted that the validity of eq 10 is not warranted outside the explored temperature range. An analogous temperature effect on molar absorptivity was reported for  $\text{CO}_2$  dissolved in water.<sup>86</sup> These results have a critical impact on the recently proposed technique for studying the thermodynamics of weak solid–gas interactions via FTIR spectroscopy (the so-called VTIR method), based on the assumption of a negligible temperature dependence of  $\epsilon$ .<sup>91</sup>

**3.2. DFT Calculations: PEI/ $\text{CO}_2$  Structures and Vibrational Spectra.** We performed quantum chemical calculations of different PEI/ $\text{CO}_2$  adducts with a 2-fold purpose: (i) to identify the most stable supramolecular complex and the preferential site of interaction on the polymer backbone; (ii) to simulate the FTIR spectrum of the adduct, thus deepening the interpretation of the spectroscopic results.

In order to look at all possible interaction sites between  $\text{CO}_2$  and PEI, several starting geometries have been tested. At first, constrained geometry optimizations, forcing the interaction between  $\text{CO}_2$  and PEI in different binding points (i.e., nitrogen atom, phenyl ring,  $\text{sp}^3$  and  $\text{sp}^2$  oxygen atoms of PEI) and different orientations, have been performed. Then, the most promising structures were fully optimized, removing all



**Table 2. Observed and Calculated Frequencies of the Relevant Normal Modes and Calculated Interaction Energies for the Investigated PEI/CO<sub>2</sub>**

	mode description	freq (calc), cm <sup>-1</sup>	freq (obs), cm <sup>-1</sup>	err %	$\Delta\nu$ (calc), cm <sup>-1</sup>	$\Delta\nu$ (obs), cm <sup>-1</sup>	$E_i$ , kJ/mol	
CO <sub>2</sub>	$\nu_2$	620.2	669	7.3	-	-	-	
	$\nu_3$	2382.6	2349	1.4	-	-	-	
	$\nu_s(\text{C=O})$	1734.0	1726	0.5	-	-	-	
PEI	$\nu_{as}(\text{C=O})$	1773.0	1779	0.3	-	-	-	
	$\nu_{as}(\text{C-O-C})$	1198.8	1214	1.2	-	-	-	
	$\nu_2'$	613.4	652	5.9	-6.8	-17	-16.9	
PEI(C=O)/CO <sub>2</sub>	$\nu_2''$	628.7 (15)	659 (7)	4.6	8.5	-10		
	$\nu_3$	2371.7	2336	1.5	-10.9	-13		
	$\nu_s(\text{C=O})$	1725.6	1722	0.2	-8.4	-4		
	$\nu_{as}(\text{C=O})$	1767.5	1776	0.5	-5.5	-3		
	$\nu_{as}(\text{C-O-C})$	1198.5	1214	1.3	-0.3	0		
	PEI(Ph)/CO <sub>2</sub>	$\nu_2'$	613.0	652	6.0	-7.2	-17	-15.8
		$\nu_2''$	628.1 (15)	659 (7)	4.7	7.9	-10	
		$\nu_3$	2370.8	2336	1.5	-11.8	-13	
		$\nu_s(\text{C=O})$	1725.5	1722	0.2	-8.5	-4	
$\nu_{as}(\text{C=O})$		1767.7	1776	0.5	-5.3	0.5		
$\nu_{as}(\text{C-O-C})$		1199.0	1214	1.2	0.2	1.2		
PEI(C-O-C)/CO <sub>2</sub>	$\nu_2'$	618.5	652	5.1	-1.7	-17	-11.5	
	$\nu_2''$	623.5 (5)	659 (7)	5.4	3.3	-10		
	$\nu_3$	2366.4	2336	1.3	-16.2	-13		
	$\nu_s(\text{C=O})$	1730.7	1722	0.5	-3.3	-4		
	$\nu_{as}(\text{C=O})$	1769.6	1776	0.4	-3.4	0.5		
	$\nu_{as}(\text{C-O-C})$	1192.0	1214	1.8	-6.8	1.2		

constraints. Only three different minima were identified: one that features CO<sub>2</sub> coordinated to the PEI carbonyl group, PEI(C=O)/CO<sub>2</sub> (Figure 4A), one where CO<sub>2</sub> coordination involves both the carbonyl and, partially, the phenyl ring, PEI(Ph)/CO<sub>2</sub> (Figure 4B), and a last one where CO<sub>2</sub> is interacting with PEI through the etheric oxygen, PEI(C-O-C)/CO<sub>2</sub> (Figure 4C). The obtained results show quite clearly that coordination of CO<sub>2</sub> to PEI preferentially occurs through the carbonyl oxygens of PEI. Even if coordination through etheric oxygens appears to be energetically possible, it is less favored, in particular, at low CO<sub>2</sub> concentrations. The PEI(C=O)/CO<sub>2</sub> minimum (see Figure 4A) shows a C=O–CO<sub>2</sub> distance of 2.77 Å and an interaction energy around -17 kJ/mol. The possibility of CO<sub>2</sub> coordination through PEI-phenyl rings was thoroughly investigated. The only stable structure that we calculated displays just a “proximity” between the CO<sub>2</sub> and the phenyl ring, with a detected average distance of 3.79 Å and a C=O–CO<sub>2</sub> distance of 2.92 Å (see Figure 4B). This structure is almost isoenergetic with the previous one (see Table 2). In fact, the slightly weakening of the C=O/CO<sub>2</sub> interaction is balanced by the proximity between the CO<sub>2</sub> molecule and the PEI phenyl ring that contributes to stabilize the structure.

A comparison between DFT-calculated spectra and their experimental counterparts (see Table 2) highlights the reliability of the QM analysis. Considering first the PEI(C=O)/CO<sub>2</sub> model, it is found that the simulated spectrum is able to capture not only the direction of the shifts induced by the interaction but also their absolute values, especially for the two carbonyl components and the  $\nu_3$  mode of CO<sub>2</sub>. For the  $\nu_3$  mode, the agreement is less satisfactory both for the peak position in the unperturbed model and for the predicted perturbation. This discrepancy has been already documented<sup>91</sup> and was ascribed to the distinct sensitivity of this vibration to the properties of the surrounding medium. However, the

simulation correctly predicts the splitting of the  $\nu_2$  signal, originally at 620 cm<sup>-1</sup>, in two components at 613–629 cm<sup>-1</sup>, due to the distortion of the linear CO<sub>2</sub> structure. The departure of the O=C=O angle ( $\beta$ ) from 180° is a characteristic of LA–LB complexes and is a sensitive measure of the interaction strength.<sup>92,93</sup> In the present case, a  $\beta$  value of 177.7° points to a moderate/weak LA–LB interaction, in comparison to the reference values for a wide number of CO<sub>2</sub>/donor complexes reported in ref 93.

The above considerations can be extended to the PEI(Ph)/CO<sub>2</sub> model. The calculated spectrum is essentially coincident with the one previously discussed, confirming that vibrational spectroscopy is unable to discriminate between the two structures. The  $\beta$  value is 178.2°, due to the weaker interaction strength.

Finally, the PEI(C-O-C)/CO<sub>2</sub> model predicts a significant perturbation of the  $\nu_{as}(\text{C-O-C})$  vibration calculated at 1199 cm<sup>-1</sup> and observed at 1214 cm<sup>-1</sup> (a *red-shift* of 7 cm<sup>-1</sup>). This effect is not detected experimentally, which confirms the negligible involvement of the etheric oxygens in LA–LB interactions.

**3.3. Atomistic Molecular Dynamics Simulations.** MD simulations have been performed to model CO<sub>2</sub> molecules inside the PEI matrix at finite temperature and at the concentrations corresponding to sorption experiments at 308.15 K, in order to directly compare simulation results with FTIR, DFT calculations, and thermodynamic theory. To this aim, we first obtained a reliable model of the PEI amorphous phase and validated it against experimentally determined density and X-ray scattering data. In order to improve statistics, quite large atomistic systems (~90 000 atoms) have been used. MD simulations of PEI amorphous phase well compare with experimental densities (1267 g/cm<sup>3</sup>, experimental range 1268–1286 g/cm<sup>3</sup>).<sup>94–97</sup> Moreover, X-ray scattering patterns, calculated from MD simulations, are in very

good agreement with experimental data (see Figure S9 of SI). Radial distribution functions (RDFs) between the carbon and oxygen atoms of CO<sub>2</sub> against the functional groups belonging to PEI chains calculated for all considered systems at different compositions are reported in Figures 5 and 6. The strongest interactions, corresponding to the highest peak in the RDF distributions, are found between the carbon (C) of carbon dioxide and the oxygen atoms (OC) of the carbonyl group. See Figure 5a for the RDFs and Figure 5d for the atom type definition. This result agrees with both FTIR experiments and DFT calculations. More in detail, the maximum in the RDF is found at ~0.3 nm (first highest peak), and the lowest minimum at ~0.5 nm. A second broader and less intense peak is found at ~0.8 nm. For a distance larger than ~1.5 nm, the probability to find an OC atom is the same as for the homogeneous bulk phase. From the RDFs reported in Figure 5a appears a non-negligible structuration for the pair of C (from carbon dioxide) and N (imide groups of PEI). As can be seen from the figure, the first peak of the C–N RDFs has a similar height to that for C–OC, but the peak position is shifted +0.2 nm with respect to the position of  $r = 0.3$  nm of the C–OC pair. This reflects, according to the molecular geometry of the imide rings, the geometrical constraint (1–3 relative positions OC and N atoms) of this atom pair. For this reason, we should consider as the strongest interaction the one corresponding to the C–OC pair. Minor differences in the RDFs are found as a function of CO<sub>2</sub> weight fraction indicating a negligible effect of CO<sub>2</sub> concentration in the explored composition range, as confirmed by FTIR measurements showing band shapes consisting of a single, sharp Lorentzian. Excepting for the relatively high structuration of C and nitrogen atom N belonging to the imide group (see Figure 5a), a weaker interaction is found for all other pairs (see panels a–g in Figure 6). Looking at the oxygen atoms (O) of carbon dioxide, we always found a weak interaction with all atoms belonging to a PEI chain (see Figure 6d–g). These results further confirm the observations gained by *time-resolved* FTIR measurements, monitoring the sorption/absorption of CO<sub>2</sub> in PEI, from which it is clear that PEI weakly interacts with the carbon dioxide (Figure S7B of the SI file).

Overall, MD simulations confirm that carbon dioxide molecules interact primarily with oxygen atoms belonging to carbonyl groups of the imide portion of PEI; this behavior is found to be short ranged (within 0.3 nm). Furthermore, in the limit of explored concentrations of carbon oxide in PEI, the strength of the interaction is insensitive to gas content. This view agrees with results coming from both FTIR spectra and DFT calculations.

**3.4. Sorption Thermodynamics of CO<sub>2</sub> in PEI: Results and Modeling.** In this section is presented the theoretical fitting of CO<sub>2</sub> sorption measurements in PEI using data obtained by gravimetry in this investigation. To the best of our knowledge, only two data sets are available in the literature near the range of pressure and temperatures investigated in the present contribution.<sup>95,96</sup> The comparison of these two literature studies with our experimental results was possible only for a limited number of data points, due to the partial overlap of the experimental conditions, resulting in a good agreement. However, since some important details on samples used in refs 95 and 96 were missing (polymer density) and since processing conditions to obtain the glassy polymer samples were different from those adopted by us, we chose to

perform the theoretical interpretation only on our experimental data.

In Figure 7 are reported the experimental sorption isotherms of CO<sub>2</sub> in PEI. The isotherms have been modeled using the NETGP-NR model. The model parameters for pure PEI and CO<sub>2</sub> have been retrieved from the literature<sup>26,33</sup> and are reported in Table 3.

**Table 3. NRHB Lattice Fluid Parameters**

	$\epsilon_h$ (J mol <sup>-1</sup> )	$\epsilon_s$ (J mol <sup>-1</sup> K <sup>-1</sup> )	$V_{sp,0}$ (cm <sup>3</sup> g <sup>-1</sup> )	$s$	ref
CO <sub>2</sub>	3468.4	-4.5855	0.79641	0.909	32
PEI	6775.3	5.503	0.7228	0.743	28

The phase pseudoequilibrium calculations require the value of the out-of-equilibrium density of the polymer,  $\rho_p$ , within the glassy mixture (see the SI file). In view of the low solubility displayed by CO<sub>2</sub> in the investigated pressure range,  $\rho_p$  is assumed to be equal to the density of the dry polymer right after the initial desorption stage that precedes a series of consecutive sorption tests.

The value of the polymer density has been assumed to be a function only of the temperature.<sup>34,35</sup> Under the assumption that the volumetric expansion coefficient,  $\alpha$ , is constant in the ranges of temperature and pressure investigated,  $\rho_p(T)$  has been calculated according to the following expression:

$$\rho_p = \rho_{p,\text{ref}} e^{-\alpha(T-T_{\text{ref}})} \quad (11)$$

using as a reference density,  $\rho_{p,\text{ref}}$  the pure polymer density at  $T_{\text{ref}} = 25$  °C.

The determination of the mean-field interaction parameter,  $k_{1p}$ , as a function of temperature, according to eq S28 reported in the SI file, has been performed by fitting concurrently all the sorption isotherms determined at several temperatures (0, 10, 18, 27, 35 °C) with the NETGP-NR model, obtaining for the interaction parameters the values  $k_{1p,0} = 0.301$  and  $a_T = -0.00100$  K<sup>-1</sup>. As shown in Figure 7 the NETGP-NR model provides an excellent fitting of the experimental sorption isotherms of CO<sub>2</sub> in PEI.

The experimental data have been re-elaborated by means of eq 4 obtaining an estimated value of  $\Delta H_1^{\text{ISOST}} = -31.1$  kJ/mol, at  $T = 18$  °C and at a value of CO<sub>2</sub> concentration equal to 0.4 [g of CO<sub>2</sub>/100 g of PEI]. Once the values of the binary interaction parameters were determined by fitting experimental sorption isotherms, we were able to predict in the same conditions, using the NETGP-NR model (eqs 2 and 3), a value  $\Delta H_1^{\text{ISOST}} = -28.3$  kJ/mol, which compares well with the value retrieved directly from the experimental data.

Moreover, we have used the NETGP-NR model (eq. 5) to estimate  $\underline{E}_{1p,0}$  at 1 K by extrapolating at this temperature the values of the model parameters calculated in the 0–35 °C range. A value equal to -18.6 kJ/mol has been obtained, which is quite close to the range of values [-15.8, -16.9] kJ/mol of the two most stable conformers determined by means of DFT calculations which mainly involve the interaction energy between one molecule of CO<sub>2</sub> and the polymer carbonyl groups, PEI(C=O)/CO<sub>2</sub>. This result points to the consistency between the thermodynamic and DFT approaches.

As further validation of the correct reproduction of carbon dioxide/PEI interaction of the proposed MD model, we calculated the excess of chemical potential of carbon dioxide in the condition of infinite dilution ( $\mu_i^{\text{ex},\infty}$ ), which is a function of

the environment polymer (solvent) interaction with the CO<sub>2</sub> (solute) using the Widom test particle insertion (TPI) method, according to ref 97. As detailed in Section S5 of the SI file, this value is compared with the corresponding independent predictive calculation provided by the NETGP-NR thermodynamic model. The excess of chemical potential calculated with the two independent methods shows a good agreement, thus validating the consistency of models in representing CO<sub>2</sub>–polymer interactions.

**3.5. Sorption Kinetics of CO<sub>2</sub> in PEI: Results and Modeling.** Values of mutual diffusivity,  $D_{12}$ , at different concentrations of absorbed CO<sub>2</sub> and at several temperatures have been determined by fitting the experimental sorption kinetics with eq 6. An example of an experimental sorption kinetic curve for the 0–100 Torr pressure step at 0 °C is reported in Figure 8, where  $\frac{M(t)}{M_\infty}$  is plotted as a function of  $\sqrt{t}$ , along with the best fitting curve provided by eq 6, from which it is evident the Fickian nature of the sorption mechanism.

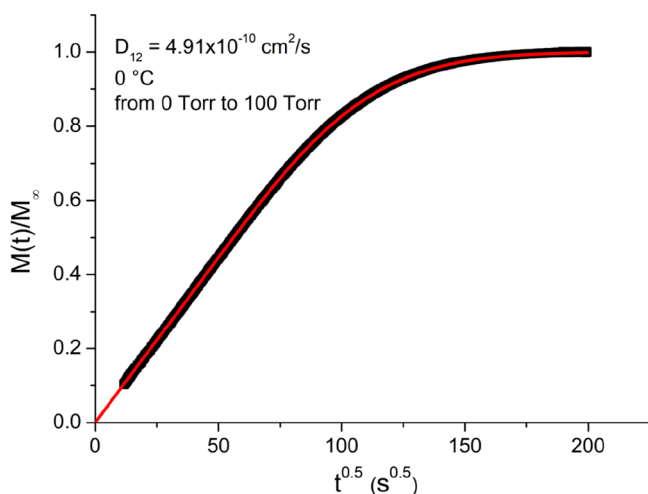


**Figure 8.** Example of CO<sub>2</sub> sorption kinetics in PEI determined gravimetrically at  $T = 0$  °C in the pressure range 0–100 Torr. Normalized mass uptake of CO<sub>2</sub> is reported as a function of square root of sorption time. The continuous red line represents the best fitting of data using eq 6.

Values of  $D_{12}$  have been determined at all the investigated temperatures, evidencing a dependence on CO<sub>2</sub> concentration. These values are reported in Figure 9 as a function of the average concentration during each sorption test at different temperatures and have been interpreted using the NETGP-NR-DM, based on eqs 7 and 8. As evident, this model provides an excellent interpretation of data. The values of best fitting parameters present in the expression of the intradiffusion coefficient are reported in Table 4.

The value of  $E_d$  and the corresponding concentration-dependent activation energy values  $E_d(1 - \sigma_c C)$  in the range of concentration investigated are significantly higher than the mean-field interaction energy per mole of penetrant,  $\bar{E}_{1p,0}$ . This is expected, since  $E_d$  represents the activation energy in the limit of zero concentration and accounts for energetic barriers to diffusion related both to the polymer–penetrant interactions and to the cohesive energy of polymer molecules, while  $\bar{E}_{1p,0}$  only accounts for penetrant–polymer interaction.

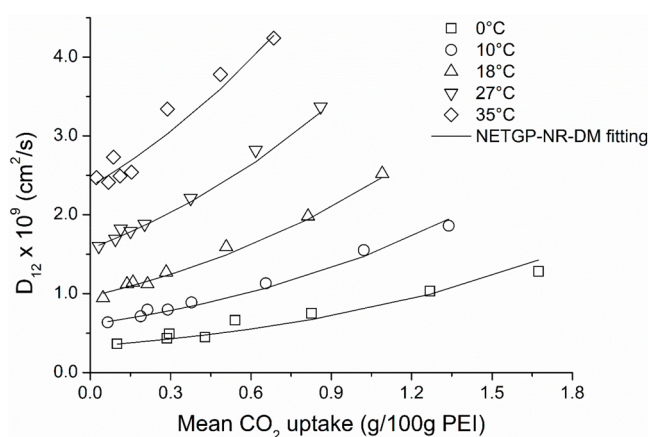


**Figure 9.** Values of mutual diffusivity for the CO<sub>2</sub>–PEI systems, obtained by fitting of the sorption kinetics data using eq 6, reported as a function of the average concentration of CO<sub>2</sub> during the sorption step.

**Table 4. CO<sub>2</sub> Intradiffusion Parameters**

$E_d$ (kJ mol <sup>-1</sup> )	$\alpha$ [dimensionless]	$D_{00}$ (cm <sup>2</sup> s <sup>-1</sup> )
39.29	2.82	0.011

## CONCLUSIONS

The description, the prediction, and the elucidation of molecular mechanisms of weak interactions between CO<sub>2</sub> and synthetic polymers are difficult, but fundamental to design efficient materials suitable for membrane-based separations ruled by solubility selectivity. The binary system made of CO<sub>2</sub> molecules absorbed in glassy PEI has been thoroughly investigated since this class of membranes is the material of choice, as a neat matrix or combined with several types of fillers, for separations of gas mixtures containing carbon dioxide. The analysis has been performed by combining DFT calculations, MD simulations, vibrational spectroscopy analysis, gravimetric sorption measurements, and statistical thermodynamics modeling. The concurrent application of these approaches provided a consistent thermodynamic and detailed atomic scale picture of the interactions.

Absorbed CO<sub>2</sub> molecules prevalently establish a relatively weak interaction with carbonyls of the imide groups of PEI as indicated by the conformational DFT investigation and confirmed by MD simulations. This conclusion is further supported by the vibrational analysis of absorbed CO<sub>2</sub> molecules (antisymmetric stretching,  $\nu_3$ , and bending,  $\nu_2$ , modes) and of the substrate spectrum ( $\nu_s(\text{C}=\text{O})$  and  $\nu_{as}(\text{C}=\text{O})$  vibrations both display a red-shift in the presence of CO<sub>2</sub>).

Based on these indications, the thermodynamics of the binary glassy PEI–CO<sub>2</sub> system has been interpreted using the NETGP-NR lattice fluid model, which does not consider the presence of strong specific interactions between the polymer and the penetrant. After concurrent fitting with the model equations of gravimetric sorption isotherms of CO<sub>2</sub> in PEI, estimates of relevant parameters related to PEI–CO<sub>2</sub> interaction energy have been obtained. In particular, we predicted theoretically the isosteric heat of sorption of CO<sub>2</sub> in PEI, which compares very well with the value determined from experimental sorption isotherms, and the interaction energy of an absorbed molecule of CO<sub>2</sub> with the surrounding polymer



matrix, which is in good agreement with the value estimated by quantum chemistry (DFT) calculations.

Finally, mutual diffusivity of CO<sub>2</sub> has been determined experimentally at several temperature and concentration values and accurately interpreted using free volume theory where the expression of the driving force for diffusion had been calculated on the basis of the expression of chemical potential of absorbed CO<sub>2</sub> provided by the NETGP-NR model.

## ■ ASSOCIATED CONTENT

### SI Supporting Information

The Supporting Information is available free of charge at <https://pubs.acs.org/doi/10.1021/acs.macromol.2c01382>.


Supplementary FTIR data details on the MD-SCF approach, on the atomistic model of PEI, and on the relaxation procedure for amorphous PEI, glass transition temperature calculations; description of the NR and NETGP-NR models; quantum chemistry/normal coordinate calculations; details on the excess of chemical potential of carbon dioxide in the condition of infinite dilution calculation (PDF)

## ■ AUTHOR INFORMATION

### Corresponding Authors

**Giuseppe Mensitieri** – Department of Materials and Production Engineering, University of Naples Federico II, 80125 Naples, Italy;  [orcid.org/0000-0001-9333-0292](https://orcid.org/0000-0001-9333-0292); Email: [mensitie@unina.it](mailto:mensitie@unina.it)

**Pellegrino Musto** – Institute for Polymers, Composites and Biomaterials, National Research Council of Italy, 80078 Pozzuoli, NA, Italy;  [orcid.org/0000-0001-6307-1410](https://orcid.org/0000-0001-6307-1410); Email: [pellegrino.musto@cnr.it](mailto:pellegrino.musto@cnr.it)

**Andrea Correa** – Department of Chemical Science, University of Naples Federico II, 80126 Napoli, Italy;  [orcid.org/0000-0003-4238-2732](https://orcid.org/0000-0003-4238-2732); Email: [andrea.correa@unina.it](mailto:andrea.correa@unina.it)


### Authors

**Giuseppe Scherillo** – Department of Materials and Production Engineering, University of Naples Federico II, 80125 Naples, Italy;  [orcid.org/0000-0003-2757-0647](https://orcid.org/0000-0003-2757-0647)

**Antonio Baldanza** – Department of Materials and Production Engineering, University of Naples Federico II, 80125 Naples, Italy

**Valerio Loianno** – Department of Materials and Production Engineering, University of Naples Federico II, 80125 Naples, Italy

**Marianna Pannico** – Institute for Polymers, Composites and Biomaterials, National Research Council of Italy, 80078 Pozzuoli, NA, Italy;  [orcid.org/0000-0001-9740-4105](https://orcid.org/0000-0001-9740-4105)

**Antonio De Nicola** – Scuola Superiore Meridionale, 80138 Napoli, Italy;  [orcid.org/0000-0002-9581-6226](https://orcid.org/0000-0002-9581-6226)

**Giuseppe Milano** – Department of Materials and Production Engineering, University of Naples Federico II, 80125 Naples, Italy

Complete contact information is available at: <https://pubs.acs.org/doi/10.1021/acs.macromol.2c01382>

### Notes

The authors declare no competing financial interest.

## ■ REFERENCES

- (1) Kontogeorgis, G. M.; Folas, G. K. *Thermodynamic Models for Industrial Applications. From Classical and Advanced Mixing Rules to Association Theories*, 1st ed.; John Wiley & Sons Ltd: Chichester, UK, 2010.
- (2) Panayiotou, C. G.; Birdi, K. S. *Handbook of Surface and Colloid Chemistry*, 3rd ed.; CRC Press Taylor and Francis Group: New York, 2009.
- (3) Iwamoto, R.; Kusanagi, H. Hydration Structure and Mobility of the Water Contained in Poly(ethylene terephthalate). *J. Phys. Chem. A* **2015**, *119* (12), 2885–2894.
- (4) Sammon, C.; Mura, C.; Yarwood, J.; Everall, N.; Swart, R.; Hodge, D. FTIR-ATR Studies of the Structure and Dynamics of Water Molecules in Polymeric Matrixes. A Comparison of PET and PVC. *J. Phys. Chem. B* **1998**, *102* (18), 3402–3411.
- (5) Davis, E. M.; Elabd, Y. A. Water Clustering in Glassy Polymers. *J. Phys. Chem. B* **2013**, *117* (36), 10629–10640.
- (6) Taylor, L. S.; Langkilde, F. W.; Zografi, G. Fourier transform Raman spectroscopic study of the interaction of water vapor with amorphous polymers. *J. Pharm. Sci.* **2001**, *90* (7), 888–901.
- (7) De Angelis, M. G.; Sarti, G. C. Solubility of Gases and Liquids in Glassy Polymers. *Annu. Rev. Chem. Biomol.* **2011**, *2*, 97–120.
- (8) Belov, N. A.; Safronov, A. P.; Yampolskii, Y. P. Inverse Gas Chromatography and the Thermodynamics of Sorption in Polymers. *Polym. Sci. Ser. A* **2012**, *54* (11), 859–873.
- (9) Galizia, M.; Chi, W. S.; Smith, Z. P.; Merkel, T. C.; Baker, R. W.; Freeman, B. D. Polymers and Mixed Matrix Membranes for Gas and Vapor Separation: A Review and Prospective Opportunities. *Macromolecules* **2017**, *50* (20), 7809–7843.
- (10) Glass, J. E. Adsorption characteristics of water-soluble polymers. I. Poly(vinyl alcohol) and poly(vinylpyrrolidone) at the aqueous-air interface. *J. Phys. Chem.* **1968**, *72* (13), 4450–4458.
- (11) Zhao, Z.-J.; Wang, Q.; Zhang, L.; Wu, T. Structured Water and Water-Polymer Interactions in Hydrogels of Molecularly Imprinted Polymers. *J. Phys. Chem. B* **2008**, *112* (25), 7515–7521.
- (12) Chiessi, E.; Cavalieri, F.; Paradossi, G. Water and Polymer Dynamics in Chemically Cross-Linked Hydrogels of Poly(vinyl alcohol): A Molecular Dynamics Simulation Study. *J. Phys. Chem. B* **2007**, *111* (11), 2820–2827.
- (13) Eslami, H.; Müller-Plathe, F. Molecular Dynamics Simulation of Water Influence on Local Structure of Nanoconfined Polyamide-6,6. *J. Phys. Chem. B* **2011**, *115* (32), 9720–9731.
- (14) Ricci, E.; Vergadou, N.; Vogiatzi, G. G.; De Angelis, M. G.; Theodorou, D. Molecular Simulations and Mechanistic Analysis of the Effect of CO<sub>2</sub> Sorption on Thermodynamics, Structure, and Local Dynamics of Molten Atactic Polystyrene. *Macromolecules* **2020**, *53*, 3669–3689.
- (15) Li, D.; Yao, J.; Wang, H. Thin Films and Membranes with Hierarchical Porosity. In *Encyclopedia of Membrane Science and Technology*, 1st ed.; Hoek, E. M. V.; Tarabara, V. V., Eds.; Wiley-Blackwell: Hoboken, NJ, USA, 2013.
- (16) Bernstein, R.; Kaufman, Y.; Freger, V. Membrane Characterization. In *Encyclopedia of Membrane Science and Technology*, 1st ed.; Hoek, E. M. V.; Tarabara, V. V., Eds.; Wiley-Blackwell: Hoboken, NJ, USA, 2013.
- (17) Brunetti, A.; Barbieri, G.; Drioli, E. Gas Separation, Applications. In *Encyclopedia of Membrane Science and Technology*, 1st ed.; Hoek, E. M. V.; Tarabara, V. V., Eds.; Wiley-Blackwell: Hoboken, NJ, USA, 2013.
- (18) Koros, W. J.; Burgess, S. K.; Chen, Z. Polymer Transport Properties. In *Encyclopedia of Polymer Science and Technology*, 4th ed.; Mark, H. F., Ed.; John Wiley & Sons: Hoboken, NJ, USA, 2015.
- (19) Koros, W. J.; Fleming, G. K.; Jordan, S. M.; Kim, T. H.; Hoehn, H. H. Polymeric membrane materials for solution-diffusion based permeation separations. *Prog. Polym. Sci.* **1988**, *13* (4), 339–401.
- (20) Dobrovskiy, A. Y.; Nazarychev, V. M.; Volgin, I. V.; Lyulin, S. V. The Transport Properties of Semi-Crystalline Polyetherimide BPDA-P3 in Amorphous and Ordered States: Computer Simulations. *Membranes* **2022**, *12*, 856.

- (21) Checchetto, R.; Scarpa, M.; De Angelis, M. G.; Minelli, M. Mixed gas diffusion and permeation of ternary and quaternary CO<sub>2</sub>/CO/N<sub>2</sub>/O<sub>2</sub> gas mixtures in Matrimid<sup>®</sup>, polyetherimide and poly(lactic acid) membranes for CO<sub>2</sub>/CO separation. *J. Membr. Sci.* **2022**, *659*, 120768.
- (22) Mannan, H. A.; Yih, T. M.; Nasir, R.; Muhktar, H.; Mohshim, D. F. Fabrication and characterization of polyetherimide/polyvinyl acetate polymer blend membranes for CO<sub>2</sub>/CH<sub>4</sub> separation. *Polym. Eng. Sci.* **2019**, *59* (S1), No. E293-E301.
- (23) Mazinani, S.; Ramezani, R.; Darvishmanesh, S.; Molelekwa, G. F.; Di Felice, R.; Van der Bruggen, B. A ground breaking polymer blend for CO<sub>2</sub>/N<sub>2</sub> separation. *J. CO<sub>2</sub> Util.* **2018**, *27*, 536–546.
- (24) Zhang, L.; Xiao, Y.; Chung, T.-S.; Jiang, J. Mechanistic understanding of CO<sub>2</sub>-induced plasticization of a polyimide membrane: A combination of experiment and simulation study. *Polymer* **2010**, *51*, 4439–4447.
- (25) Ewing, A. V.; Gabrienko, A. A.; Semikolenov, S. V.; Dubkov, K. A.; Kazarian, S. G. How Do Intermolecular Interactions Affect Swelling of Polyketones with a Differing Number of Carbonyl Groups? An In Situ ATR-FTIR Spectroscopic Study of CO<sub>2</sub> Sorption in Polymers. *J. Phys. Chem. C* **2015**, *119*, 431–440.
- (26) de Nicola, A.; Correa, A.; Milano, G.; La Manna, P.; Musto, P.; Mensitieri, G.; Scherillo, G. Local Structure and Dynamics of Water Absorbed in Polyetherimide: A Hydrogen Bonding Anatomy. *J. Phys. Chem. B* **2017**, *121* (14), 3162–3176.
- (27) Mensitieri, G.; Scherillo, G.; Panayiotou, C.; Musto, P. Towards a predictive thermodynamic description of sorption processes in polymers: the synergy between theoretical EoS models and vibrational spectroscopy. *Materials Science & Engineering Reports R* **2020**, *140C*, 100525.
- (28) Mensitieri, G.; Scherillo, G.; La Manna, P.; Musto, P. Sorption thermodynamics of CO<sub>2</sub>, H<sub>2</sub>O and CH<sub>3</sub>OH in a glassy polyetherimide: a molecular perspective. *Membranes* **2019**, *9*, 23.
- (29) Musto, P.; La Manna, P.; Cimino, F.; Mensitieri, G.; Russo, P. Morphology, Molecular Interactions and H<sub>2</sub>O Diffusion in a Poly(lactic-acid)/Graphene composite: a Vibrational Spectroscopy Study. *Spectrochimica Acta Part A: Molecular and Biomolecular Spectroscopy* **2019**, *218*, 40–50.
- (30) Scherillo, G.; La Manna, P.; Musto, P.; Mensitieri, G. Water sorption thermodynamics in glassy polymers endowed with hydrogen bonding interactions'. *SCIENCE CHINA Physics, Mechanics & Astronomy* **2020**, *63*, 247012.
- (31) Scherillo, G.; Sanguigno, L.; Galizia, M.; Lavorgna, M.; Musto, P.; Mensitieri, G. Non-equilibrium compressible lattice theories accounting for hydrogen bonding interactions: Modelling water sorption thermodynamics in fluorinated polyimides. *Fluid Phase Equilib.* **2012**, *334*, 166–188.
- (32) Panayiotou, C.; Pantoula, M.; Stefanis, E.; Tsvintzelis, I.; Economou, I. G. Nonrandom Hydrogen-Bonding Model of Fluids and Their Mixtures. 1. Pure Fluids. *Ind. Eng. Chem. Res.* **2004**, *43* (20), 6592–6606.
- (33) Panayiotou, C.; Tsvintzelis, I.; Economou, I. G. Nonrandom Hydrogen-Bonding Model of Fluids and Their Mixtures. 2. Multi-component Mixtures. *Ind. Eng. Chem. Res.* **2007**, *46* (8), 2628–2636.
- (34) Doghieri, F.; Sarti, G. C. Nonequilibrium Lattice Fluids: A Predictive Model for the Solubility in Glassy Polymers. *Macromolecules* **1996**, *29*, 7885–7896.
- (35) Sarti, G. C.; Doghieri, F. Predictions of the solubility of gases in glassy polymers based on the NELF model. *Chem. Eng. Sci.* **1998**, *53* (19), 3435–3447.
- (36) Musto, P.; La Manna, P.; Pannico, M.; Mensitieri, G.; Gargiulo, N.; Caputo, D. Molecular interactions of CO<sub>2</sub> with the CuBTC metal organic framework: an FTIR study based on two-dimensional correlation spectroscopy. *J. Mol. Struct.* **2018**, *1166*, 326–333.
- (37) Pierleoni, D.; Minelli, M.; Scherillo, G.; Mensitieri, G.; Loianno, V.; Bonavolontà, F.; Doghieri, F. 'Analysis of a Polystyrene-Toluene System through 'Dynamic' Sorption Tests: Glass Transitions and Retrograde Vittrification'. *J. Phys. Chem. B* **2017**, *121* (42), 9969–9981.
- (38) Frisch, M. J.; Trucks, G. W.; Schlegel, H. B.; Scuseria, G. E.; Robb, M. A.; Cheeseman, J. R.; Scalmani, G.; Barone, V.; Mennucci, B.; Petersson, G. A.; Nakatsuji, H.; Caricato, M.; Li, X.; Hratchian, H. P.; Izmaylov, A. F.; Bloino, J.; Zheng, G.; Sonnenberg, J. L.; Hada, M.; Ehara, M.; Toyota, K.; Fukuda, R.; Hasegawa, J.; Ishida, M.; Nakajima, T.; Honda, Y.; Kitao, O.; Nakai, H.; Vreven, T.; Montgomery, J. A., Jr.; Peralta, J. E.; Ogliaro, F.; Bearpark, M.; Heyd, J. J.; Brothers, E.; Kudin, K. N.; Staroverov, V. N.; Kobayashi, R.; Normand, J.; Raghavachari, K.; Rendell, A.; Burant, J. C.; Iyengar, S. S.; Tomasi, J.; Cossi, M.; Rega, N.; Millam, J. M.; Klene, M.; Knox, J. E.; Cross, J. B.; Bakken, V.; Adamo, C.; Jaramillo, J.; Gomperts, R.; Stratmann, R. E.; Yazyev, O.; Austin, A. J.; Cammi, R.; Pomelli, C.; Ochterski, J. W.; Martin, R. L.; Morokuma, K.; Zakrzewski, V. G.; Voth, G. A.; Salvador, P.; Dannenberg, J. J.; Dapprich, S.; Daniels, A. D.; Farkas, O.; Foresman, J. B.; Ortiz, J. V.; Cioslowski, J.; Fox, D. *J. Gaussian 09, Revision A.1*; Gaussian, Inc.: Wallingford, CT, 2009.
- (39) Ditchfield, R.; Hehre, W. J.; Pople, J. A. Self-Consistent Molecular Orbital Methods. 9. Extended Gaussian-type basis for molecular-orbital studies of organic molecules. *J. Chem. Phys.* **1971**, *54*, 724–737.
- (40) Hariharan, P. C.; Pople, J. A. Accuracy of AH equilibrium geometries by single determinant molecular-orbital theory. *Mol. Phys.* **1974**, *27*, 209–14.
- (41) Francl, M. M.; Pietro, W. J.; Hehre, W. J.; Binkley, J. S.; DeFrees, D. J.; Pople, J. A.; Gordon, M. S. Self-Consistent Molecular Orbital Methods. 23. A polarization-type basis set for 2nd-row elements. *J. Chem. Phys.* **1982**, *77*, 3654–65.
- (42) Rassolov, V. A.; Pople, J. A.; Ratner, M. A.; Windus, T. L. 6-31G\* basis set for atoms K through Zn. *J. Chem. Phys.* **1998**, *109*, 1223–29.
- (43) Rassolov, V. A.; Ratner, M. A.; Pople, J. A.; Redfern, P. C.; Curtiss, L. A. 6-31G\* Basis Set for Third-Row Atoms. *J. Comput. Chem.* **2001**, *22*, 976–84.
- (44) Zhao, Y.; Truhlar, D. G. The M06 suite of density functionals for main group thermochemistry, thermochemical kinetics, non-covalent interactions, excited states, and transition elements: two new functionals and systematic testing of four M06-class functionals and 12 other functionals. *Theor. Chem. Acc.* **2008**, *120*, 215–41.
- (45) Zhao, Y.; Truhlar, D. G. A new local density functional for main-group thermochemistry, transition metal bonding, thermochemical kinetics, and noncovalent interactions. *J. Chem. Phys.* **2006**, *125*, 1–18.
- (46) Scott, A. P.; Radom, L. Harmonic Vibrational Frequencies: An Evaluation of Hartree-Fock, Møller-Plesset, Quadratic Configuration Interaction, Density Functional Theory and Semiempirical Scale Factors. *J. Phys. Chem.* **1996**, *100*, 16502–16530.
- (47) Boys, S. F.; Bernardi, F. Calculation of Small Molecular Interactions by Differences of Separate Total Energies - Some Procedures with Reduced Errors. *Mol. Phys.* **1970**, *19*, 553–579.
- (48) Jorgensen, W. L.; Tirado-Rives, J. The OPLS [Optimized Potentials for Liquid Simulations] Potential Functions for Proteins, Energy Minimizations for Crystals of Cyclic Peptides and Crambin. *J. Am. Chem. Soc.* **1988**, *110* (6), 1657–1666.
- (49) Correa, A.; De Nicola, A.; Scherillo, G.; Loianno, V.; Mallamace, D.; Mallamace, F.; Ito, H.; Musto, P.; Mensitieri, G. A Molecular Interpretation of the Dynamics of Diffusive Mass Transport of Water within a Glassy Polyetherimide. *Int. J. Mol. Sci.* **2021**, *22* (6), 2908–2912.
- (50) De Nicola, A.; Kawakatsu, T.; Milano, G. Generation of Well-Relaxed All-Atom Models of Large Molecular Weight Polymer Melts: A Hybrid Particle-Continuum Approach Based on Particle-Field Molecular Dynamics Simulations. *J. Chem. Theory Comput.* **2014**, *10* (12), 5651–5667.
- (51) De Nicola, A.; Munaò, G.; Grizzuti, N.; Auriemma, F.; De Rosa, C.; Sevinck, A.; Milano, G. Generation of Well Relaxed All Atom Models of Stereoregular Polymers: A Validation of Hybrid Particle-Field Molecular Dynamics for Polypropylene Melts of Different Tacticities. *Soft Mater.* **2020**, *18* (2–3), 228–241.



- (52) Milano, G.; Kawakatsu, T. Hybrid Particle-Field Molecular Dynamics Simulations for Dense Polymer Systems. *J. Chem. Phys.* **2009**, *130* (21), 214106–12.
- (53) Milano, G.; Kawakatsu, T. Pressure Calculation in Hybrid Particle-Field Simulations. *J. Chem. Phys.* **2010**, *133* (21), 214102–23.
- (54) Zhao, Y.; De Nicola, A.; Kawakatsu, T.; Milano, G. Hybrid Particle-Field Molecular Dynamics Simulations: Parallelization and Benchmarks. *J. Comput. Chem.* **2012**, *33* (8), 868–880.
- (55) Andersen, H. C. Molecular Dynamics Simulations at Constant Pressure and/or Temperature. *J. Chem. Phys.* **1980**, *72* (4), 2384–2393.
- (56) Li, M.; Liu, X. Y.; Qin, J. Q.; Gu, Y. Molecular dynamics simulation on glass transition temperature of isomeric polyimide. *Express Polymer Letters*. **2009**, *30* (10), 665–675.
- (57) Pan, R.; Liu, X. Y.; Zhang, A.; Gu, Y. Molecular simulation on structure-property relationship of polyimides with methylene spacing groups in biphenyl side chain. *Comput. Mater. Sci.* **2007**, *39* (4), 887–895.
- (58) Liang, T.; Yang, X.; Zhang, X. Prediction of polyimide materials with high glass transition temperature. *Journal of Polymer Science Part B Polymer Physics*. **2001**, *39* (19), 2243–2251.
- (59) Wen, C.; Liu, B.; Wolfgang, J.; Long, T. E.; Odle, R.; Cheng, S. Determination of glass transition temperature of polyimides from atomistic molecular dynamics simulations and machine-learning algorithms. *J. Polym. Sci.* **2020**, *58* (11), 1521–1534.
- (60) Nazarychev, V. M.; Larin, S. V.; Lyulin, A. V.; Dingemans, T.; Kenny, J. M.; Lyulin, S. V. Atomistic Molecular Dynamics Simulations of the Initial Crystallization Stage in an SWCNT-Polyetherimide Nanocomposite. *Polymers* **2017**, *9* (10), 548–556.
- (61) Martínez, L.; Andrade, R.; Birgin, E. G.; Martínez, J. M. PACKMOL: A Package for Building Initial Configurations for Molecular Dynamics Simulations. *J. Comput. Chem.* **2009**, *30* (13), 2157–2164.
- (62) Van Der Spoel, D.; Lindahl, E.; Hess, B.; Groenhof, G.; Mark, A. E.; Berendsen, H. J. C. GROMACS: Fast, Flexible, and Free. *J. Comput. Chem.* **2005**, *26* (16), 1701–1718.
- (63) Berendsen, H. J. C.; Postma, J. P. M.; van Gunsteren, W. F.; DiNola, A.; Haak, J. R. Molecular Dynamics with Coupling to an External Bath. *J. Chem. Phys.* **1984**, *81* (8), 3684–3690.
- (64) Hess, B.; Bekker, H.; Berendsen, H. J. C.; Fraaije, J. G. E. M. LINCS: A Linear Constraint Solver for Molecular Simulations. *J. Comput. Chem.* **1997**, *18* (12), 1463–1472.
- (65) Coleman, B. D.; Gurtin, M. E. Thermodynamics with Internal State Variables. *J. Chem. Phys.* **1967**, *47*, 597–613.
- (66) Astarita, G.; Sarti, G. C. Modern Thermodynamics in Chemical Engineering and Chemistry. I. *Chem. and Industr.* **1975**, *57* (10), 680–688.
- (67) Astarita, G. *Thermodynamics: An Advanced Textbook for Chemical Engineers*; Plenum Press: New York, 1989.
- (68) Astarita, G. *An Introduction to Nonlinear Continuum Thermodynamics*; SpA Editrice di Chimica: Milan, 1975.
- (69) De Donder, Th.; Van Rysselberghe, P. *Thermodynamic Theory of Affinity*; Stanford University Press, 1936.
- (70) Buoles, S.; Sandler, S. I.; Xiong, R. Isothermic heats of gas and liquid adsorption. *Langmuir* **2013**, *29*, 10416–10422.
- (71) Crank, J. *The Mathematics of Diffusion*, 2nd ed.; Clarendon Press: Oxford, 1975.
- (72) Stannett, V. Simple Gases. In *Diffusion in Polymers*; Crank, J.; Park, G. S., Eds.; Academic Press: London, Chapter 2, 1968.
- (73) Fujita, H. Organic Vapors above the Glass Transition Temperature. In *Diffusion in Polymers*; Crank, J.; Park, G. S., Eds.; Academic Press; London, Chapter 3, 1968.
- (74) Alentiev, A. Yu.; Shantarovich, V. P.; Merkel, T. C.; Bondar, V. I.; Freeman, B. D.; Yampolskii, Yu. P. Gas and Vapor Sorption, Permeation, and Diffusion in Glassy Amorphous Teflon AF1600. *Macromolecules* **2002**, *35*, 9513–9522.
- (75) Yampolskii, Yu.; Shishatskii, S.; Alentiev, A.; Loza, K. Correlations with and prediction of activation energies of gas permeation and diffusion in glassy polymers. *J. Membr. Sci.* **1998**, *148*, 59–69.
- (76) Vrentas, J. S.; Duda, J. L. Diffusion in polymer-solvent systems: I. Re-examination of the free-volume theory. *J. Polym. Sci. Polym. Phys. Ed.* **1977**, *15*, 403–416.
- (77) Vrentas, J. S.; Duda, J. L. Diffusion in polymer-solvent systems: II. A predictive theory for the dependence of the diffusion coefficient on temperature, concentration and molecular weight. *J. Polym. Sci. Polym. Phys. Ed.* **1977**, *15*, 417–439.
- (78) Duda, J. L.; Zielinski, J. M. Free-volume theory. In *Diffusion in Polymers*; Neogi, P., Ed.; Marcel Dekker Inc.: New York, 1996; Chapter 3, pp 143–172.
- (79) Di Maio, E.; Iannace, S.; Mensitieri, G. Mass transport of low molecular weight compounds in polymer. In *Foaming with Supercritical Fluids*; Elsevier, Amsterdam, 2021; Chapter 6, pp 179–230.
- (80) Loianno, V.; Baldanza, A.; Scherillo, G.; Jamaledin, R.; Musto, P.; Mensitieri, G. A Hyphenated Approach Combining Pressure-Decay and In Situ FT-NIR Spectroscopy to Monitor Penetrant Sorption and Concurrent Swelling in Polymers. *Ind. Eng. Chem. Res.* **2021**, *6*, 5494–5503.
- (81) Turner, Bandwidths, J. J. *Handbook of Vibrational Spectroscopy*; Chalmers, J. M.; Griffiths, P. R., Eds.; Wiley, 2002; Vol. 1, pp 101–127.
- (82) Pitha, J.; Norman-Jones, R. A Comparison of Optimization Methods for Fitting Curves to Infrared Band Envelopes. *Can. J. Chem.* **1966**, *44* (24), 3031–3050.
- (83) Döge, G.; Yarwood, J. Infrared and Raman studies on molecular dynamics in liquid. *Studies in physical and theoretical chemistry* **1991**, *74*, 274–363.
- (84) Ouillon, R.; Breuillard, C. Raman and infrared spectroscopic study of the molecular dynamics of N<sub>2</sub>O in inert solvents: I. Rotational relaxation. *Mol. Phys.* **1981**, *44*, 363–380.
- (85) James, D.; Frost, R. L. Relaxation processes in aqueous solution: a Raman spectral study of hydrogen bonded interactions. *J. Chem. Soc. Farad. Disc.* **1977**, *64*, 48–54.
- (86) Maiella, P.; Schoppelrei, J.; Brill, T. Spectroscopy of hydrothermal reactions. Part XI: Infrared absorptivity of CO<sub>2</sub> and N<sub>2</sub>O in water at elevated temperature and pressure. *Appl. Spectrosc.* **1999**, *53*, 351–355.
- (87) Griffiths, J. E. Molecular reorientational motion in liquid acetonitrile: Raman band shapes, diffusion constants and activation energy of reorientation. *J. Chem. Phys.* **1973**, *59*, 751–758.
- (88) Kazarian, S. G.; Vincent, M. F.; Bright, F. V.; Liotta, C. L.; Eckert, C. A. Specific intermolecular interaction of carbon dioxide with polymers. *J. Am. Chem. Soc.* **1996**, *118*, 1729–1736.
- (89) Musto, P.; Karasz, F. E.; MacKnight, W. J. Hydrogen bonding in polybenzimidazole/polyimide systems: a Fourier-transform infrared investigation using low-molecular-weight monofunctional probes. *Polymer* **1989**, *30*, 1012–1021.
- (90) Falk, M.; Miller, A. G. Infrared spectrum of carbon dioxide in aqueous solution. *Vib. Spectrosc.* **1992**, *4*, 105–108.
- (91) Garrone, E.; Areán, C. O. Variable temperature infrared spectroscopy: a convenient tool for studying the thermodynamics of weak solid-gas interactions. *Chem. Soc. Rev.* **2005**, *34*, 846–857.
- (92) Pastore, Carbone, M. G.; Musto, P.; Pannico, M.; Brauer, A.; Scherillo, G.; Mensitieri, G.; Di Maio, E. Raman line imaging of poly( $\epsilon$ -caprolactone)/carbon dioxide solutions at high pressures: a combined experimental and computational study for interpreting intermolecular interactions and free-volume effects. *J. Phys. Chem. B* **2016**, *120*, 9115–9131.
- (93) Jamroz, M. H.; Dobrowolski, J. C.; Bajdor, K.; Borowiak, M. A. Ab-Initio Study of the Nu(Co<sub>2</sub>) Mode in Eda Complexes. *J. Mol. Struct.* **1995**, *349*, 9–12.
- (94) Jonas, A. M.; Ivanov, D. A.; Yoon, D. Y. The Semicrystalline Morphology of Poly(ether-ether- ketone) Blends with Poly (ether-imide). *Macromolecules* **1998**, *31* (16), 5352–5362.
- (95) Kumazawa, H.; Wang, J.-S.; Fukuda, T.; Sada, E. Permeation of carbon dioxide in glassy poly (ether imide) and poly (ether ether ketone) membranes. *J. Membr. Sci.* **1994**, *93*, 53–59.



(96) Lopez-Gonzalez, M.; Compan, V.; Saiz, E.; Riande, E.; Guzman, J. Effect of the upstream pressure on gas transport in poly(ether-imide) films. *J. Membr. Sci.* **2005**, *253*, 175–181.

(97) Widom, B. Some Topics in the Theory of Fluids. *J. Chem. Phys.* **1963**, *39*, 2808–2812.

## Recommended by ACS

### Autonomous Search for Polymers with High Thermal Conductivity Using a Rapid Green–Kubo Estimation

Akihiro Nagoya, Takanori Takeno, *et al.*

APRIL 25, 2022  
MACROMOLECULES

READ 

### Salt Destabilization of Cationic Colistin Complexation within Polyanionic Microgels

Xixi Xiao, Matthew Libera, *et al.*

FEBRUARY 14, 2022  
MACROMOLECULES

READ 

### Effects of Ionic Group Distribution on the Structure and Dynamics of Amorphous Polymer Melts

Supun S. Mohottalalage, Dvora Perahia, *et al.*

DECEMBER 23, 2021  
MACROMOLECULES

READ 

### Sequence Effects on the Salt-Enhancement Behavior of Polyelectrolytes Adsorption

Qihui Chang and Jian Jiang

JANUARY 24, 2022  
MACROMOLECULES

READ 

Get More Suggestions >